CAPITAL UNIVERSITY OF SCIENCE AND TECHNOLOGY, ISLAMABAD


# Finite Element Implementation and Analysis of a Localized Deformation Microstructure through FreeFEM++

by

Zarafshan Azeem

A thesis submitted in partial fulfillment for the degree of Master of Philosophy

in the

Faculty of Computing
Department of Mathematics

2025

*I dedicate my thesis to*

*my beloved family, friends specially*

***My Mother(Yasmeen Akhtar)***,

*A determined and aristocratic embodiment who educate me to belief in ALLAH,*

*believe in hard work and that so much could be done with little,*

***My Father(Muhammad Azeem)***

*I quote the remarkable words of Hadith,*

*"A father gives his child nothing better than an education."*


# CERTIFICATE OF APPROVAL

Finite Element Implementation and Analysis of a Localized Deformation Microstructure through FreeFEM++

by

Zarafshan Azeem

(Registration No: MMT233005)

## THESIS EXAMINING COMMITTEE

| S. No. | Examiner | Name | Organization |
|---|---|---|---|
| (a) | External Examiner | Dr. Rashid Mahmood | Namal University Mianwali |
| (b) | Internal Examiner | Dr. Samina Batool | CUST, Islamabad |
| (c) | Supervisor | Dr. Muhammad Sabeel Khan | CUST, Islamabad |

Dr. Muhammad Sabeel Khan
Thesis Supervisor
April, 2025

Dr. Muhammad Sagheer
Head
Dept. of Mathematics
April, 2025

Dr. M. Abdul Qadir
Dean
Faculty of Computing
April, 2025

# *Author's Declaration*

I, **Zarafshan Azeem** hereby state that my MPhil thesis titled "**Finite Element Implementation and Analysis of a Localized Deformation Microstructure through FreeFEM++**" is my own work and has not been submitted previously by me for taking any degree from Capital University of Science and Technology, Islamabad or anywhere else in the country/abroad.

At any time if my statement is found to be incorrect even after my graduation, the University has the right to withdraw my MPhil Degree.

**(Zarafshan Azeem)**

Registration No: MMT233005

# *Plagiarism Undertaking*

I solemnly declare that research work presented in this thesis titled "**Finite Element Implementation and Analysis of a Localized Deformation Microstructure through FreeFEM++**" is solely my research work with no significant contribution from any other person. Small contribution/help wherever taken has been duly acknowledged and that complete thesis has been written by me.

I understand the zero tolerance policy of the HEC and Capital University of Science and Technology towards plagiarism. Therefore, I as an author of the above titled thesis declare that no portion of my thesis has been plagiarized and any material used as reference is properly referred/cited.

I undertake that if I am found guilty of any formal plagiarism in the above titled thesis even after award of MPhil Degree, the University reserves the right to withdraw/revoke my MPhil degree and that HEC and the University have the right to publish my name on the HEC/University website on which names of students are placed who submitted plagiarized work.

**(Zarafshan Azeem)**

Registration No: MMT233005

# *Acknowledgement*

In the name of **ALLAH**, who is the most merciful and beneficent, created the universe and blessed the mankind with intelligence and wisdom to explore its secret. I would like to express my heart felt gratitude and immeasurable respect to my supervisor **Dr. Muhammad Sabeel Khan** for his passionate interest, willingness help, superb guidance and inspiration throughout this investigation.

I am extremely grateful to my all teachers for their encouragement and emphasis on striving for excellence when teaching mathematics. I would like to acknowledge the CUST for providing me such a favourable environment to this research.

I must express my very profound gratitude to my dear parents and family members for providing me with unfailing support and continuous encouragement throughout my years of study. Also I express my special thanks to my beloved sister **Alia** and brother **Mujtaba Azeem** for their patience on not getting my attention during my very busy schedule in writing this thesis.

Finally, I want to express my gratitude to my Friends who encouraged me throughout my MPhil research. I am grateful to my fellow researchers at CUST for valuable discussions on this research. I have enjoyed working alongside them in a pleasant working environment.

**(Zarafshan Azeem)**

Registration No: MMT233005

Type text here

# *Abstract*

In this thesis, we present a relaxed continuum model for granular structures. The mathematical model presented is described in the form of a relaxed energy potential in the Cosserat continuum. This energy potential is afterwards used to derive the constitutive response of the elastic material under consideration. The model presented enables us to capture the localized deformation bands that appear within the granular structure under applied stress. Granular bands appear in the structured material due to localized deformations in the medium that arises due to fine scale oscillations of the underlying microstructure in the elastic medium. The presented model within the elastic regime is afterwards transformed into finite element setting and implemented by using the open source code FreeFEM++. To solve the system of equations, iterative solver i.e the conjugate gradient method is utilized. The implemented code is used to analyze the model for two test problems in structural mechanics. The first problem is the compression of a granular slab under pure compression and the second problem is the Couette shear cell under pure rotation. The results are displayed for both scenarios where they demonstrate on the development of microstructure and associated shear band formation.

# Contents

# List of Figures

# List of Tables

# Abbreviations

| | |
|---|---|
| **BCT** | Boltzmann Continuum Theory |
| **CCT** | Cosserat Continuum Theory |
| **CPFE** | Crystal Plasticity Finite Element Method |
| **FEM** | Finite Element Method |
| **GFEM** | Galerkin Finite Element Method |

# Symbols

| | |
|---|---|
| $\varphi$ | Micro-rotation vector field |
| $E$ | Modulus of elasticity |
| $W$ | Relaxed energy |
| $t_u$ | Traction force |
| $t_\varphi$ | Traction moments |
| $t$ | Time |
| $V$ | Velocity vector field |
| $\nabla$ | Gradient operator |
| $\mu$ | Classical elastic shear modulus |
| $\mu_c$ | Cosserat shear modulus |
| $\epsilon$ | Cauchy tensor |
| $\kappa$ | Curvature strain tensor |
| $\bar{\lambda}$ | Cosserat material dilatancy parameter |
| $\bar{\mu_c}$ | Coupled shear modulus |
| $u$ | $x$-component of velocity |
| $v$ | $y$-component of velocity |
| $\beta$ | Viscoelastic parameters |
| $\lambda$ | Classical dilatancy parameter |
| $\phi_i$ | Basis functions |
| $w_i$ | Weight functions |
| $\Omega$ | Material domain |
| $\sigma$ | classical stress tensor |

# Chapter 1

# Introduction and Literature Survey

In the analysis of microstructured materials, energy relaxation techniques have been used for the considerable number of engineering problems or applications in a wide field of mechanics, especially in elasticity, elasto-plasticity and plasticity. To understand about these, here are few studies: linear problems in elastic-plastic design [1], for phase transformations [2] and within a Cosserat continuum, microstructures analyzed through relaxed energy methods [3]. A relaxed energy envelope that reflects the non-quasi-convex energy potential must always be created when simulating the mechanical behavior of these materials, so these studies [4] and [5] are in the literature where computation of these energies was possible.

In energy minimization issues, quasi-convex energy envelopes are utilized in practical scenarios, for instance, to the situations with oscillating gradients of the minimizing deformations that are thin at the scales. The oscillations that occur at small scales in the minimizing deformations are responsible for the appearance of material microstructures. The mechanics of microstructures in materials, that are granular, is a complex and intriguing topic, especially in accordance with Cosserat continuum theory (CCT) [6]. One class of these models, which are based on phase-field techniques, continuum thermodynamics, and crystal plasticity, allows for the explanation of many physical mechanisms and their interactions during the growth

of microstructures at the continuum level[7]. There are continuum mechanics techniques that are used in constitutive relations that exhibit a significant impact of such nonlinearities as yield stress, dilatancy, and density gradients [8]. Also, the dynamical form of non-local granular fluidity can be incorporated into the three-dimensional material point technique, a suitable solver for simulating granular flow, using a numerical methodology presented in a hyperelasticity framework. This method ensures energy conservation because it is consistent with thermodynamics [9]. The significance of deformation under non-isothermal conditions is highlighted with respect to its role in the characterisation of the thermomechanical behaviour of materials, particularly in the context of energy geostructures. The development of a new model to improve the prediction of microstructure evolution during forming operation while integrating remeshing capabilities with crystal plasticity finite element (CPFE) is presented here [10] and using large-deformation models to improve microstructural prediction can increase the production yield, strength, and longevity of lightweight forged parts. Moreover, deformation rate depends upon stress-strain relations of material as discussed in[11]. The modeling of stress-strain constitutive relations in solids endowed with internal angular degree of freedom would be achievable using the Cosserat elasticity theory[12] in contrast to Boltzmann continuum theory (BCT), which states that the stress at a material point is dependent entirely on the strain at that same point [13]. So, this is enough to explain the microstructural behavior of the granular material in terms of nonspecific attributes of each grain of micro-rotation concerning its macro-rotation. This allows for independent rotational degrees of freedom at each material point.

Furthermore, rotation of grains forms the central aspect of the kinematics of grain-scale deformation in granular materials. Although such computational capacities are already available today, description at continuum level is efficient and still required for capturing the deformation of these materials at large length scales. It is, however, based on continuum model for their rotations [14]. Thus, it is indeed a broadly accepted theory that has been successfully deployed for microstructural modelling of granular materials, according to literature such as [15]. This work uses the Cosserat continuum theory to describe the deformation of granular materials.

Additionally, in order to examine the uses of CCT, the reader is directed to [16], [17] and the references therein. Here is another study that uses the material point technique of continuum mechanics to study the impacts of its constitutive development on the flow behavior of granular materials. It also enhances the material point method's algorithm to represent various granular flow states [18]. At macro and micro scales, the impact of packing structure on heat transfer in granular media is investigated using different methods [19]. In addition to it, granular micromechanics approach is also used to examine the critical state in which deformation occurs without change of volume [20]. Also, the instability aspect in granular structural problem is linked to the emergence of a load limit, triggered by significant nonlinear geometric effects [21].

In addition, the mechanisms of localization of plastic deformation under different strain rates tend to change and are highly related to the choice of deformation mechanisms in metallic materials for various strain rates [22] and deformation by gradation extrusion [23]. Rotations of particles constitute an important mechanism that has an impact on macroscopic behavior in granular materials. For a better understanding of the various aspects of rotations of particles in granular material deformation mechanisms, the reader is directed to [24]. The failure behavior of granular materials is influenced by microscopic parameters, such as contact stiffness and its characteristic length, the reader is encourages to [25]. Efforts towards observing and predicting the broad micros in granular materials along with localized deformations have been made both experimentally and numerically [26]. In addition, machine learning is also being utilized to examine the effect of microstructures of granular materials [27] and to predict the constitutive response of granular soils [28]. The finite-element simulation analyzes how anisotropy affects the localization pattern and bearing capacity of geostructures [29] and also finite element implementation is used for modelling several classes of hetrogeneous media, the reader is directed to [30] and [31].

Although there are few variational methods in the literature that can calculate and observe localized deformations and extended microstructures simultaneously in a single model, these phenomena have been examined as bifurcation events in

the past. This research, therefore, suggests a sophisticated computational algorithm that is used in the finite element method to forecast localized deformations, extended microstructure formations, and microstructural phenomena of granular material in the special setting of a variational approach in Cosserat elasticity. There are many characteristics of the exact quasi-convex energy envelopes in certain physical situations can also be studied using this method.

## 1.1 Thesis Contribution

We introduce a relaxed continuum model for granular structures in this thesis. A relaxed energy potential in the Cosserat continuum serves as a description of the mathematical model that is being presented. The constitutive response of the elastic material is then determined by using the energy potential. We can capture the localized deformation bands that emerge within the granular structure when stress is applied. Localized medium deformations brought on by fine-scale oscillations of the underlying microstructure in the elastic medium cause granular bands to form in the structured material. The model that is shown in the elastic regime is then converted to a finite element setup and put into practice using the FreeFEM++ open source code. There are two structural mechanics test problems that are analyzed using the implemented code. The compression of a granular slab under pure compression is the first issue, and the Couette shear cell under pure rotation is the second. The outcomes are displayed for both scenarios in which the developed code demonstrates the development of the microstructure and associated shear band generation.

## 1.2 Objectives

The objectives of this investigation include:

- To present a relaxed continuum model in elasticity theory for prediction on plastic deformation.

- To formulate the relaxed energy for the granular materials within Cosserat continuum that can lead to microstructure observation within these materials.
- To develop a finite element model of the relaxed mathematical model in the Cosserat continuum.
- To develop a weak formulation of the presented strong form of the relaxed continuum model within Cosserat continuum.
- To implement the developed weak formulation using an open source code FreeFEM++.
- To analyze the implemented code for two test model problems. First problem is the formation of shear band formation in a granular slab under compressive load. The second problem is the formation of the localized deformation bands in the Couette shear cell.

## 1.3 Thesis Layout

This thesis is further composed of the following chapters:

- **Chapter 2** illustrates basic theoretical concepts related to vector and tensor calculus. Some important properties in vectors and tensors are also described. Furthermore, some basic fundamental concepts in theory of elasticity are explained and also microstructures of granular materials are discussed briefly. Moreover, relaxed energies of the material are given.
- In **Chapter 3**, relaxed version of Cosserat continuum model is described. Also, this model is applied on granular materials. Relaxed energies corresponding to functions and variational formulation of the model are also discussed.
- In **Chapter 4**, formulation of Finite Element Method is described along with numerical algorithm, used to solve the problem. In this chapter numerical

execution of the model in which after the weak formulation of model, its component form is given and its simulations using FreeFEM++ are discussed. In addition to it, numerical algorithm of the model is also presented.

- After required simulations, in **Chapter 5** that model is applied on two test problems to visualize the localized deformation bands that become visible within the granular structure under applied stress. These bands appear because of fine scale oscillations of the microstructure in the elastic medium. This is implemented using the open source code software FreeFEM++. In first problem, compression of a granular slab under pure compression and in second problem the Couette shear cell under pure rotation is analyzed.

- **Chapter 6** comprises of conclusion and future work.

The work's references are numerated in Bibliography.

# Chapter 2

# Mathematical Concepts and Theoretical Background

In this chapter we are going to discuss fundamental concepts, definitions, governing laws and theories related to the structural dynamics.

## 2.1 Fundamental Concepts in Vector and Tensor Calculus

In this section, some fundamental concepts related to vectors and tensors are introduced.

### 2.1.1 Vector Calculus

#### 2.1.1.1 Vector

A physical quantity that is fully characterized by both its magnitude and direction, such as force, velocity, momentum and acceleration, is called **vector** designated by **f,v,P,a**.
It is a directed line element in space.

In three-dimensional Euclidean space, any vector $\mathbf{u}$ can be represented as a linear combination of basis vectors $e_1, e_2$ and $e_3$ i.e.

$$\mathbf{u} = u_1 e_1 + u_2 e_2 + u_3 e_3,$$

where $u_1, u_2$ and $u_3$ are three real numbers which are uniquely determined rectangular components of vector along the given directions $e_1, e_2$ and $e_3$ respectively in the figure.

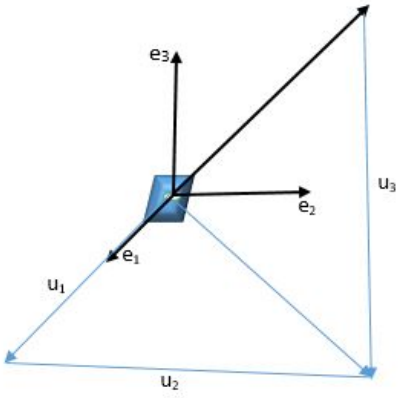


FIGURE 2.1: Components of vector $\mathbf{u}$ [32]

#### 2.1.1.2 Vector Field

"A vector field is a function that assigns a vector to each point in a subset of space. Mathematically, $\mathbf{X} : A \to \mathbb{R}^n$ is a function where $(A \subseteq \mathbb{R}^n)$ is a domain such that for every point x ∈ A, X(x)∈ $\mathbb{R}^n$ is a vector"[33].
In 3D, a vector field can be given as a vector function of the form

$$\mathbf{X}(x, y, z) = (X_1(x, y, z), X_2(x, y, z), X_3(x, y, z)) .$$

#### 2.1.1.3 Length of a Vector

The square root of $\mathbf{u} \cdot \mathbf{u}$ defines the length, or norm of a vector $\mathbf{u}$, which is a non-negative real number, i.e.

$$|u| = (\mathbf{u} \cdot \mathbf{u})^{\frac{1}{2}} \geq 0, \quad |\mathbf{u}|^2 = \mathbf{u} \cdot \mathbf{u}.$$

#### 2.1.1.4 Dot Product

The scalar, or dot of **u** and **v** is defined as

$$\mathbf{u} \cdot \mathbf{v} = |u||v| cos\theta(u, v), \qquad 0 \leq \theta(u, v) \leq \pi$$

where $\theta$ is the angle between two vectors **u** and **v**. This scalar product gives us a scalar quantity with some properties given below

$$\mathbf{u} \cdot \mathbf{v} = \mathbf{v} \cdot \mathbf{u}, \qquad \mathbf{u} \cdot \mathbf{o} = 0,$$

$$\mathbf{u} \cdot (a\mathbf{v} + b\mathbf{w}) = a(\mathbf{u} \cdot \mathbf{v}) + b(\mathbf{u} \cdot \mathbf{w}),$$

$$\mathbf{u} \cdot \mathbf{u} > 0 \quad \text{if}\, \mathbf{u} \neq \mathbf{o} \quad \text{and} \quad \mathbf{u} \cdot \mathbf{u} = 0 \quad \text{if} \quad \mathbf{u} = \mathbf{o}.$$

#### 2.1.1.5 Divergence of a Vector Field

It is defined as the dot product of a vector operator $\nabla$ and any smooth vector field which gives us a scalar field and denoted by div**u**, given below

$$\text{div}\mathbf{u} = \nabla \cdot \mathbf{u} = \frac{\partial u_p}{\partial x_q} \mathbf{e}_p \cdot \mathbf{e}_q = \frac{\partial u_p}{\partial x_q} \delta_{pq} = \frac{\partial u_p}{\partial x_p}.$$

In Euclidean space $\mathbb{R}^3$ it can be written as,

$$\text{div}\mathbf{u} = \frac{\partial u_1}{\partial x_1} + \frac{\partial u_2}{\partial x_2} + \frac{\partial u_3}{\partial x_3}.$$

#### 2.1.1.6 Deformation Gradient

It is defined as

$$\mathbf{F}(\mathbf{X}, t) = \frac{\partial \chi(\mathbf{X}, t)}{\partial \mathbf{X}} = \text{Grad}\, \mathbf{x}(\mathbf{X}, t),$$

where the quantity F is a measure of deformation called deformation gradient. Hence, during a certain motion $\chi$, the material curve **X** deforms into a spatial curve **x**.

#### 2.1.1.7 Gradient of a Vector Field

A vector field's gradient or derivative is referred to as a tensor field. It is indicated by grad**u**, which is given as below

$$\text{grad}\mathbf{u} = \frac{\partial u_p}{\partial x_q}\mathbf{e}_p\mathbf{e}_q.$$

In matrix notation,

$$\nabla\mathbf{u} = \begin{bmatrix} \frac{\partial u_1}{\partial x_1} & \frac{\partial u_1}{\partial x_2} & \frac{\partial u_1}{\partial x_3} \\ \frac{\partial u_2}{\partial x_1} & \frac{\partial u_2}{\partial x_2} & \frac{\partial u_2}{\partial x_3} \\ \frac{\partial u_3}{\partial x_1} & \frac{\partial u_3}{\partial x_2} & \frac{\partial u_3}{\partial x_3} \end{bmatrix}.$$

### 2.1.2 Tensor Calculus

#### 2.1.2.1 Tensor

"Let V be a finite- dimensional vector space over a field (usually $\mathbb{C}$ or $\mathbb{R}$). A tensor of type (r, s) is a multilinear map:

$$T : \underbrace{V^* \times ... \times V^*}_{r\ times} \times \underbrace{V \times ... \times V}_{s\ times} \to \mathbb{R}.$$

This means a tensor takes r covectors from dual space $V^*$ and s vectors from V and returns a scalar, and is multilinear in all arguments.

- Rank or order of the tensor is r+s.
- (r, s) is the type of the tensor."[34]

These are basically those mathematical concepts that take the idea of scalars and vectors to greater dimensions.

A tensor is an n-dimensional matrix. It is an extension of vectors, matrices, and scalars to higher dimensions. A scalar is a 0-dimensional tensor and a vector is a 1-dimensional tensor.

#### 2.1.2.2 Tensor Field

A tensor field is a function mapping every point in a region of mathematical space (usually Euclidean space or manifold) or of the physical space to a tensor. A second order tensor field A(x) with components $A_{pq}(x)$ is expressed as

$$A(x) = A_{pq}(x)\mathbf{e}_p\mathbf{e}_q.$$

Moreover, a tensor field is a set of tensors associated with every point in space. It follows that a scalar field is a zeroth-order tensor field represented by $\phi(\mathbf{x})$, where $\mathbf{x}$ is a position vector in space and a vector field is a first-order tensor field represented by $a_i(\mathbf{x})$.

#### 2.1.2.3 Scalar Product of Tensor and Vector

**A** and **B** are two second-order tensors, and their dot product is also a second-order tensor. It is denoted by **AB** and follows

$$(\mathbf{AB})\mathbf{u} = \mathbf{A}(\mathbf{Bu}),$$

for all vectors **u**.

#### 2.1.2.4 Tensor Product

"The tensor product or the dyad of the vectors **u** and **v** is denoted by $\mathbf{u} \otimes \mathbf{v}$. It is a second order tensor which linearly transforms a vector **w** into a vector with the direction of **u**."[32] and followed by the rule

$$(\mathbf{u} \otimes \mathbf{v})\mathbf{w} = \mathbf{u}(\mathbf{v} \cdot \mathbf{w}),$$

where

$$\mathbf{u} \otimes \mathbf{v} = u_i v_j.$$

A dyadic is basically a linear combination of dyads with other scaler coefficients and also formed by basis. In general,

$$\mathbf{A} = \mathbf{u} \otimes \mathbf{v} + \mathbf{w} \otimes \mathbf{x}.$$

Furthermore, the dyad is not commutative, i.e. $\mathbf{u} \otimes \mathbf{v} \neq \mathbf{v} \otimes \mathbf{u}$.

#### 2.1.2.5 Trace of a Tensor

The trace of a tensor $\mathbf{A}$ is a scalar which is denoted by tr$\mathbf{A}$ as given below

$$\text{tr}\mathbf{A} = A_{ii} = A_{11} + A_{22} + A_{33},$$

where $A_{11}, A_{22}$ and $A_{33}$ are diagnol entries of matrix.

#### 2.1.2.6 Double Dot Product

The double contraction of a tensor $\mathbf{A}$ with the tensor $\mathbf{B}$ gives a scalar, specified by two dots, denoted by $\mathbf{A}$:$\mathbf{B}$ and is given below

$$\mathbf{A} : \mathbf{B} = A_{pq}B_{mn}e_p \otimes e_q : e_m \otimes e_n = A_{pq}B_{mn}.$$

It is also defined in terms of trace by

$$\mathbf{A} : \mathbf{B} = \text{tr}(\mathbf{A}^T\mathbf{B}).$$

#### 2.1.2.7 Norm of a Tensor

The norm of a tensor $\mathbf{A}$ is a non-negative real number and is defined by the square root of $\mathbf{A}$:$\mathbf{A}$. It is denoted by $|A|$ i.e.

$$|A| = (\mathbf{A} : \mathbf{A})^{\frac{1}{2}} \geq 0.$$

#### 2.1.2.8 Deviatoric Part of Tensor

The deviatoric part of a tensor is $\mathbf{A}$ is denoted by dev$\mathbf{A}$ and is given as

$$\text{dev}\mathbf{A} = \mathbf{A} - \frac{1}{d}(\text{tr}\mathbf{A})\mathbf{I} \quad ,$$

$d$ is the dimension of a tensor.

#### 2.1.2.9 Symmetric and Asymmetric Tensor

A tensor $\mathbf{A}_{ij}$ is a symmetric tensor, if $\mathbf{A}_{ij} = \mathbf{A}_{ji}$, where $\mathbf{A}_{ji}$ is the tranpose of $\mathbf{A}_{ij}$ and asymmetric tensor, if $\mathbf{A}_{ij} = \mathbf{-A}_{ji}$.

Any tensor $\mathbf{A}$ can always be decomposed into a symmetric and asymmetric tensor, here denoted by sym$\mathbf{A}$ and asy$\mathbf{A}$, respectively. Hence,

$$\text{sym}\mathbf{A} = \frac{1}{2}(\mathbf{A} + \mathbf{A}^T), \qquad \text{asy}\mathbf{A} = \frac{1}{2}(\mathbf{A} - \mathbf{A}^T).$$

Therefore, $\mathbf{A}$ = sym$\mathbf{A}$+asy$\mathbf{A}$.

#### 2.1.2.10 Divergence and Gradient of a Tensor Field

The divergence of a tensor field is defined as the dot product of a vector operator $\nabla$ and any smooth tensor field(second-order) $\mathbf{A}$(x) which gives us a vector field and denoted by div$\mathbf{A}$, given below

$$\text{div}\mathbf{A} = \frac{\partial A_{pq}}{\partial x_q}\mathbf{e}_p.$$

The gradient of any second order tensor field is defined to be a third order tensor field and we can write

$$\text{grad}\mathbf{A} = \nabla \otimes \mathbf{A} = \frac{\partial \mathbf{A}_{pq}}{\partial x_r}\mathbf{e}_p \otimes \mathbf{e}_q \otimes \mathbf{e}_r.$$

#### 2.1.2.11 Third Order Tensor

The third order tensor, denoted by **E** and is given below

$$\mathbf{E} = E_{pqr} e_p \otimes e_q \otimes e_r.$$

is known as permutation tensor.

#### 2.1.2.12 Divergence Theorem

Assume that **u**(x) and **A**(x) are any smooth vector and tensor fields defined on a closed surface with volume v and on a convex three-dimensional region in physical space, respectively. Then for **u** and **A**, we have

$$\int_s \mathbf{u} \cdot \mathbf{n} ds = \int_v \text{div}\mathbf{u} dv,$$

$$\int_s \mathbf{A} \cdot \mathbf{n} ds = \int_v \text{div}\mathbf{A} dv,$$

where **n** is the unit vector normal to the surface s, ds and dv are infinitesimal surface and volume elements, respectively.

The divergence theorem is the important transformation of volume integral into a surface integral. Hence, similar results hold for higher order tensors.

## 2.2 Spaces

### 2.2.1 $\mathbf{L}^p-$Spaces

"Let $\Omega \subseteq \mathbb{R}^n$ be a measurable set and let $1 \leq p \leq \infty$. The space $L^p(\Omega)$ is the set of measurable functions $f : \Omega \to \mathbb{R}$ such that the p-th power of the absolute value

is integrable such as,

$$L^p(\Omega) = \left\{ f : \Omega \to \mathbb{R} \quad \text{is measurable} \,\middle|\, \int_\Omega |f(x)|^p dx \, < \infty \right\}.$$

Each $L^p(\Omega)$ with norm such as

$$||f||_{L^p} = \left( \int_\Omega |f(x)|^p dx \right)^{\frac{1}{p}},$$

is a banach space".[35]

### 2.2.2 Sobolev Space

"Let $\Omega \subseteq \mathbb{R}^n$ be an open set. The sobolev space $W^{k,p}(\Omega)$, where $k \in \mathbb{N}$ and $1 \leq p \leq \infty$, is the space of all functions u $\in L^p(\Omega)$ means functions with integrable p-th power, whose weak derivatives up to order k also belong to $L^p(\Omega)$.

Formally,

$$W^{k,p}(\Omega) = \{u \in L^p(\Omega) : D^\alpha u \in L^p(\Omega), \forall \ |\alpha| \leq k\},$$

where $\alpha = (\alpha_1, ....\alpha_n)$ is a multi-index,

$D^\alpha u = \dfrac{\partial^{|\alpha|} u}{\partial x_1^{\alpha_1} ....\partial x_n^{\alpha_n}}$ is a weak derivative,

and $|\alpha| = \alpha_1 + ..... + \alpha_n$.

When p = 2, the space $W^{k,2}(\Omega)$ is denoted by $H^k(\Omega)$ with the inner product:

$$\langle u, v \rangle = \sum_{|\alpha| \leq 1} \int_\Omega D^\alpha u(x) D^\alpha v(x) dx.$$

forms a Hilbert space."[36]

## 2.3 Basic Concepts in Material Science

### 2.3.1 Elastic Materials

Elastic materials are materials that return to their original shape after being deformed when external forces are removed. Their behavior is governed by elasticity theory, which describes how materials deform under stress and recover their original configuration upon unloading. There are several types of elastic materials.

1. **Linear Elastic Materials**:
   Linear elastic materials follow Hooke's law with a linear relationship between stress and strain. Such materials are characterized by material constants such as the Young's modulus $E$(stiffness) and the Poisson's ratio $\nu$ (lateral contraction under axial loading). Some common examples of such materials are: metals (at small strains), concrete, ceramics (under small loads).

2. **Nonlinear Elastic Materials**:
   Nonlinaer elastic materials are the materials whose stress-strain relation is not linear, but deformation is still reversible. Such materials are governed by a more complex strain energy function. Examples of such materials include: rubber, soft biological tissues, and some polymers.

3. **Hyperelastic Materials (Green Elasticity)**:
   These materials are a special type of nonlinear elastic materials where stress derives from a potential energy function $W(F)$ (strain energy density). These materials are used in large deformation problems like rubber-like materials and soft tissues. Some common models within hyperelastic materials include: Neo-Hookean model, Mooney-Rivlin model, and Ogden model

#### 2.3.1.1 Stress and Strain

Stress can simply be defined as internal force per unit area within a material.

$$\text{stress} = \frac{\text{internal force}}{\text{area}}.$$

Its SI unit is $Nm^{-2}$. The deformation of an object or a medium caused by stress. The amount that describes such deformation is known as strain. It is expressed as a fractional change in length (caused by the tensile stress) as well as in volume or geometry. It has no unit.

#### 2.3.1.2 Energy of Material

The energy of a material is that energy stored in a material due to bonding and atomic configuration and the arrangement of its particles.

### 2.3.2 Granular Material

A granular material is a type of multiphased material comprising a high-density assembly of closely packed solid particles that are surrounded by gas or liquid. Since the volume fraction of solids compared with the volume fraction of fluids is very high, the particles are in closer contact with each other.

Sand, rice, coffee grounds, ball bearings, snow, nuts, coal, and salt are examples of granular materials.

#### 2.3.2.1 Microstructures

Microstructure is the small sized structure in a material which denotes the structure of the made surface of the material as exposed by an optical microscope at least 25 times.

The microstructure of a material whether a metal, polymer, ceramic, or composite, can have a strong influence on physical properties such as strength, toughness, ductility, hardness, corrosion resistance, high temperature and low temperature behavior, or wear resistance.

Microstructure within granular materials demands importance about how it would predict the mechanical and transport properties like resistance against loading and deformation.

#### 2.3.2.2 Deformations

The occurrence of a change in shape or size from its normal position is usually called deformation, which may either be induced by the application of some forces or a temperature change. It is usually caused by forces such as:

1. **Tensile Force**.

   It refers to tensile strength, which measures the amount of force, a material can endure when being stretched or pulled before it breaks.

2. **Compressive Force**.

   It is the force which acts to squeeze an object, causing it to become compacted. It is opposite of tensile strength, which refers to a material's ability to endure compression.

3. **Shear Force**.

   A force that acts in a direction parallel to a surface or a planar cross section of an object, such as the air pressure exerted along the front of an airplane wing. It causes a structural member to deform or curve.

4. **Bending Force**.

   A bending force refers to a load that is exerted on a section of material at a specific distance from a fixed point.

5. **Torsion Force**.

   It refers to the strain or angular deformation that occurs when a material is twisted. It is quantified by the angle through which a specific section is rotated from its original, equilibrium position.

#### 2.3.2.3 Types of Deformations

In structural mechanics, deformation refers to the change in shape or size of a structure due to applied forces, thermal effects, or other external factors. Deformations can be classified based on various criteria, such as magnitude, nature of

strain, and material behavior. Based on the nature of strain in the material the deformation is further characterized into the following.

1. **Elastic Deformation**:

   It is fully reversible deformation material returns to its original shape after unloading. This deformation mehanism is governed by Hooke's law in small strains and hyperelasticity in large strains.
   Examples of such deformation includes: Steel under small loads, rubber under moderate stretching.

2. **Plastic Deformation**:

   It is irreversible deformation wherein the material does not return to its original shape after unloading. It is caused by yielding in metals beyond the elastic limit. This type of deformation is common in metal forming (forging, rolling) and crash impact scenarios.

3. **Viscoelastic Deformation**:

   It is time-dependent deformation where material behavior has both elastic (recoverable) and viscous (time-dependent) components. These type of deformatin is seen in polymers, biological tissues, and asphalt.

Based on magnitude of deformation it is further characterized into small and large strain deformation.

1. **Small Deformation (Infinitesimal Strain Theory)**:

   In small deformation it is assumed that displacements and strains are very small (typically less than 1% strain). The strain tensor is linearized, leading to simpler mathematical models. This small strain theory is used in linear elasticity for structures like bridges, buildings, and beams under normal operating conditions.

2. **Large Deformation (Finite Strain Theory)**:

   Large strain theory deals with large displacements, rotations, and strains.

This deformation theory requires nonlinear strain measures like the Green-Lagrange strain tensor. This theory is used in rubber-like materials, biological tissues, and crash simulations.

The other modes of deformation are metal fatigue, compressive failure and fracture. The metal fatigue is mainly in the ductile metals. Metal fatigue has been a frequent cause of failures before the very understanding of the process became known. Compressive failure is applied to bars, columns, etc., and causes the shortening of these. By loading a structural object or specimen, one enhances the compressive stress until it reaches its compressive strength. Fracture is probably irreversible. All the materials will eventually fracture under sufficient force.

#### 2.3.2.4 Localized Deformation in Granular Materials

It is a slow and settled phenomenon caused by movement of particles when they are subjected to a constant load. The nature of localized deformation in granular materials is influenced by:

1. Loading or unloading conditions
2. Grain size
3. Specimen density

#### 2.3.2.5 Displacement

It is the shortest distance between the starting and final points of an object, including the direction of travel from the start to the endpoint. It's a vector quantity.

#### 2.3.2.6 Displacement Field

A vector field

$$\mathbf{V}(\mathbf{X}, t) = \mathbf{x}(\mathbf{X}, t) - \mathbf{X}$$

represents the displacement field and it is related to the position in undeformed configuration '**X**' to the deformed configuration '**x**' at time t (see Figure 2.2). The material description (Lagrangian form) is characterized by the displacement field, which depends on both time and the reference position. In the Eulerian version of the spatial description, the displacement field, represented by the symbol **v**, depends on time t and the current position. We may write it as

$$\mathbf{v}(\mathbf{x}, t) = \mathbf{x} - \mathbf{X}(\mathbf{x}, t)$$

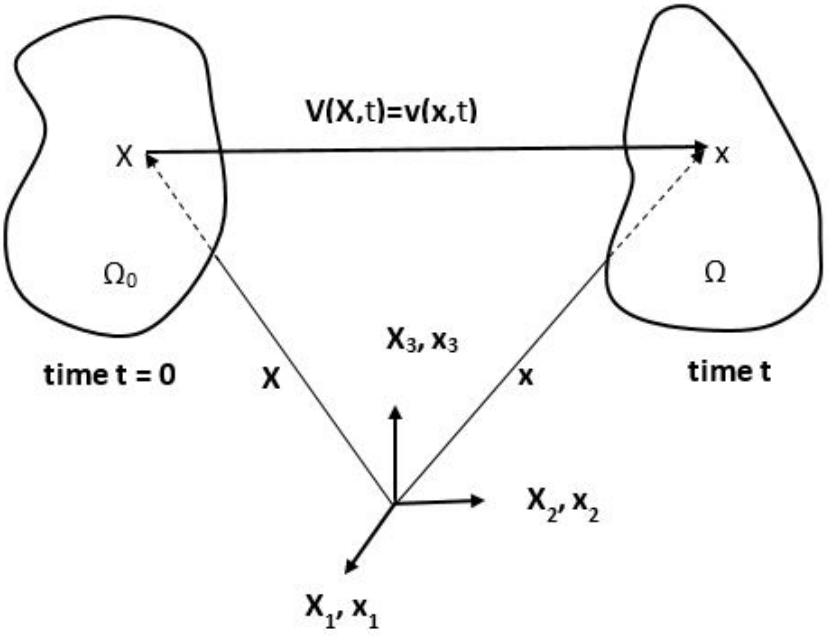


FIGURE 2.2: Displacement field **V**[32]

### 2.3.3 Energies in Material

#### 2.3.3.1 Convex Energy

Let $F : \mathbb{R}^n \to \mathbb{R}$ be an energy function. Then we can say that $F$ is convex iff for all $x$, $y \in \mathbb{R}^n$ and for all $t \in [0, 1]$,

$$F(tx + (1-t)y) \leq tF(x) + (1-t)F(y).$$

It shows the lowest energy phases (or phase combinations) for a given composition in a material system. It is used in structural analysis to calculate stress and strain fields in structures defined by convex strain energy.

#### 2.3.3.2 Quasi-convex Energy Envelope

A quasi-convex energy envelope (QCE) is the largest quasiconvex function which stays below or touches a given function. The QCE gives a representation for the convex hull of every level set of a given function.

A function **f** is quasiconvex iff for all x,y $\in \Omega$ which is convex set X and all $t \in [0, 1]$,

$$f(tx + (1 - t)y) \leq max\{f(x), f(y)\}.$$

#### 2.3.3.3 Relaxed Energy

In continuum mechanics, the concept of relaxed energy arises when dealing with materials that exhibit non-convex energy functions, phase transitions, microstructure formation, or singularities such as fractures.

Relaxation is a mathematical framework used to define a well-posed energy functional when the original energy functional is ill-posed or leads to non-physical solutions. There are many materials, especially in elasticity and plasticity, that have non-convex strain energy densities. This non-convexity leads to instabilities and microstructure formation, meaning the material undergoes phase transitions or fine-scale oscillations (e.g., twinning in crystals). Classical energy minimization may fail because it prefers highly oscillatory solutions. Relaxation replaces the original, possibly non-convex energy density $W(F)$ (as a function of the deformation gradient $F$ with its convex or quasi-convex envelope). The relaxed energy function provides a well-posed minimization problem that accounts for microstructures instead of excluding them. In the context of hyperelasticity, the relaxed energy $W_{relax}(F)$ is obtained via the quasi-convex envelope of $W(F)$.

## 2.4 Continuum Theories

### 2.4.1 Cauchy Continuum Theory

The Cauchy continuum theory is the classical framework of continuum mechanics, formulated by Augustin-Louis Cauchy in the early 19th century. It describes the behavior of materials by assuming that they are continuous (i.e., without discrete particles) and can be characterized solely by displacement and stress fields. Some of the fundamental concepts in the Cauchy continuum theory are given as below.

1. Continuity Assumption: The material is treated as a continuous medium, meaning properties vary smoothly without discrete gaps or particles. No microstructure effects (e.g., rotations of individual particles) are considered.

2. Degrees of Freedom: Each material point has three translational degrees of freedom (displacement in $x$,$y$,$z$). Rotational degrees of freedom are not independent—they are derived from displacement gradients.

3. Cauchy's Stress Tensor: The stress tensor in the Cauchy continuum is symmetric.

4. Governing Equations: The governing equations include the balance of linear momentum (Newton's second law) and the balance of angular momentum. The balance of angular momentum leads to the conclusion that the Cauchy stress tensor is symmetric.

5. Strain-displacement Relations: Deformation is described by the strain tensor in terms of displacement gradients.

#### 2.4.1.1 Limitations of Cauchy Continuum Theory

Following are some limitations of Cauchy continuum theory.

1. Does not account for microstructure effects (e.g., fiber orientations in composites, grain interactions in metals).

2. No independent rotational degrees of freedom.

3. No couple stresses (moments caused by internal forces).

For materials where such effects matter, Cosserat or micropolar continuum theories are needed.

### 2.4.2 Cosserat Continuum Theory

Cosserat continuum theory is an extension of classical continuum mechanics that accounts for microrotations and couple stresses in addition to standard displacement and force measures. It is particularly useful for modeling materials with microstructure, such as granular media, liquid crystals, and metamaterials. Some of the key features of Cosserat continuum theory are:

#### 2.4.2.1 Additional Degrees of Freedom

Unlike classical elasticity, where a material point only has translational degrees of freedom, the Cosserat continuum also allows for rotational degrees of freedom at every point.

#### 2.4.2.2 Couple stresses

In addition to the usual Cauchy stress tensor, the Cosserat theory introduces a couple stress tensor, which represents internal moments acting within the material.

#### 2.4.2.3 Asymmetric stress tensor

The classical Cauchy stress tensor is symmetric in conventional mechanics, but in Cosserat theory, it can be asymmetric due to the presence of couple stresses. The governing equations in Cosserat continumm theory includes the linear momentum balance which includes forces and classical stresses and the angular momentum

balance which includes couple stresses and micro-rotations. Cosserat continuum theory has many interesting applications. It is used in modeling behavior of materials like: granular materials (sand, powders), biological tissues (bone, cartilage), metamaterials with engineered microstructure, liquid crystals and complex fluids.

## 2.5 Basics of Finite Element Method

The Finite Element Method (FEM) actually comprises a powerful numerical technique, widely established for solving issues of engineering and mathematical physics, especially with complex structures or systems where analytical solutions prove difficult or impossible to obtain. Such applications abound in the structural analysis, heat transfer, fluid mechanics, and many more.

### 2.5.1 Formulation of FEM

The formulation of FEM model is based on the following methods:

- **Direct method**
- **Variational method**
- **Weighted residuals**

#### 2.5.1.1 Weighted Residual Method

It is a useful method for finding approximate solutions when the physical problem is described by a differential equation of this form

$$\mathcal{L}u = f, \tag{2.1}$$

where $f$ is known function, $u$ represent dependent variable and it is considered as unknown function, $\mathcal{L}$ shows differential operator for spatial derivative of $u$.

Using weighted residual method, an approximate solution or trial solution $\widetilde{u}(x)$ will be supposed, which satisfy boundary conditions. Since $\widetilde{u}$ is an approximate solution, so it will not satisfies the differential equation (2.1).

$$R(\widetilde{u}(x)) = \mathcal{L}\widetilde{u} - f \neq 0, \tag{2.2}$$

where

$$\widetilde{u}(x) = \sum_{p=1}^{m} u_p \phi'_p(x), \tag{2.3}$$

and

$$\widetilde{u}(x) = u_1\phi'_1(x) + u_2\phi'_2(x) + u_3\phi'_3(x) + ... + u_m\phi'_m(x).$$

The functions $\phi'_p$ are used as basis functions. As the function space $\phi'$ has finite dimensions, in general the expression (2.3) cannot satisfy the differential equation (2.1) in the domain for each point. This implies that the approximate solution or trial solution $\widetilde{u}$ cannot be same like $u$ (exact solution). By increasing the value of $m$, the approximate solution becomes close to the exact solution. From residual (2.2), by finding a way to make this residual small or approximately zero, the approximated solution of BVP can be evaluated. In finite element method (FEM), the approximate solution can be obtained by making suitable number of weighted integrals of residual over the domain $\Omega$ is

$$\int_{\Omega} wRd\Omega = 0, \tag{2.4}$$

where $w$= $\{w_p; p = 1, 2, ..., m\}$ is the suitable collection of weighting functions, which shows that obtained approximated solution is for m being finite.

$$w(x) = \sum_{p=1}^{m} w_p\psi_p(x) = w_1\psi_1(x) + w_2\psi_2(x) + ... + w_m\psi_m(x), \tag{2.5}$$

where $\psi_p(x)$ are "known test functions" and $w_p$ are "undetermined coefficients".

By using (2.5) in (2.4), we get

$$[A]\mathbf{u} = \mathbf{F},$$

as a system of algebraic equations. By solving above system for $m-$unknowns, $u_p^{'}s$ is provided after a suitable weight function $w$ is selected.

#### 2.5.1.2 Galerkin Finite Element Method

This is a Finite Element Analysis technique which uses "Galerkin weighted residual method" to get variational formulation of continuous problem for each individual element. These elements are the subdomains of the whole physical domain $\Omega$.

### 2.5.2 Numerical Procedure for FEM

#### 2.5.2.1 Problem Definition and Governing Equations

Define the problem and the geometry, along with the properties of the material, boundary conditions, and external loads or forces. Write down governing differential equations, which describe the physical phenomenon (e.g. equilibrium equations for mechanics, heat conduction equation for thermal problems).

#### 2.5.2.2 Discretization of the Domain (Mesh Generation)

The very first step in FEM is dividing the domain of the problem into smaller, manageable pieces (elements) - this is called meshing.

A single element is typically a simple shape (for example, a triangle or quadrilateral for 2D, tetrahedron or hexahedron for 3D), and the whole collection of these form a mesh. The finer the mesh, the more accurate the results, but at the cost of increased computation time.

#### 2.5.2.3 Selection of Element Type and Formulation

Select the right kind of element as per the problem: 1D, 2D, 3D, beam, shell, solid, etc. Then develop or apply the element shape functions which describe the variation of the solution within the element (typically with respect to polynomial functions).

#### 2.5.2.4 Assembly of the Global System of Equations

Each element has its own local set of equations. These local equations are derived from the governing differential equations, and the individual element equations must be assembled into a global system that describes the entire structure or domain.

This is done by considering the interaction between adjacent elements and ensuring the continuity of the solution across element boundaries.

#### 2.5.2.5 Application of Boundary Conditions

Apply boundary conditions (e.g., fixed supports, applied loads, temperature conditions, etc.) to the global system of equations. This will modify the global stiffness matrix and force vector. Boundary conditions are usually applied by adjusting the global matrices to reflect the constraints.

#### 2.5.2.6 Finding Solution to System of Equations

The next step is to solve the algebraic (mostly linear) system created, which solves for unknowns i.e displacement, temperature, or other quantities depending on the application.
The system tends to get quite large with time and therefore doesn't allow direct methods such as Gaussian elimination or LU decomposition but iterative solver such as conjugate gradient method instead.

#### 2.5.2.7 Result Processing and Results Interpretation

The solution obtained (for example, the displacement field, stress, strain, temperature distribution) is subject to post processing into a visible form. The process includes plotting the results (e.g., contour plots for stresses or displacements), deriving quantities such as strain from displacement or stress from strain, and checking the solution for its accuracy or convergence.

#### 2.5.2.8 Validation and Verification

At this stage, the verification of the final outcomes remains necessary. This could mean comparing FEM solutions against experimental data, as most of the time, with analytical solutions when it comes to simpler problems (benchmark tests).

## 2.6 Implementation in FreeFEM++

### 2.6.1 Structure of FreeFEM++.

FreeFEM++ is a widely used software platform designed for solving partial differential equations (PDEs) through finite element methods. Its structure consists of several key components that collaborate to define the problem, find a solution, and visualize the outcomes.

Here's an overview of its main structure:

#### 2.6.1.1 Script-based Approach:

FreeFEM++ operates mainly through scripts, where users create scripts (usually with a .edp extension) to outline their problem. These scripts resemble programming code and detail:

- Mesh Generation

- Boundary Conditions
- PDE Formulation
- Variational Problem Setup
- Solution Procedure
- Output Visualization

#### 2.6.1.2 Finite Element Space:

In FreeFEM++, solutions are approximated using finite element methods. Users establish finite element spaces based on the mesh and the type of elements (e.g., P1, P2) to approximate the solution.
- Mesh: Defined over a domain (e.g., 1D, 2D, 3D). It can be created manually or imported from external files.
- Finite element spaces: These spaces represent the solution space (e.g., piecewise linear functions, quadratic, etc.) and are defined on the mesh.

#### 2.6.1.3 Problem Definition:

Variational formulation: The partial differential equation (PDE) is reformulated into a variational form. FreeFEM++ utilizes these variational forms to transform the differential equation into a weak form that can be solved. Boundary Conditions: The script specifies the boundary conditions, which can be Dirichlet, Neumann, or Robin.

#### 2.6.1.4 Solvers:

FreeFEM++ employs linear algebra solvers to address the system of equations that arise from the discretization of the PDE. It offers:

-Direct solvers such as LU decomposition

-Iterative solvers including conjugate gradient (CG) and GMRES

#### 2.6.1.5 Functions and Operators:

FreeFEM++ includes a range of predefined functions and operators for:

- Defining integrals and derivatives
- Assembling matrices (like stiffness matrices and load vectors)
- Interpolating data
- Post-processing and visualization.

#### 2.6.1.6 Parallel Computing:

FreeFEM++ enables parallel computing for handling large-scale problems by running multiple processes and employing domain decomposition techniques.

#### 2.6.1.7 Post-Processing/Visualization:

FreeFEM++ provides users with the ability to visualize results in both 2D and 3D. This can be achieved through its built-in plotting functions or by exporting data to external software like ParaView or VTK for more sophisticated visualization options.

# Chapter 3

# Relaxed Continuum Model

Relaxed continuum modeling in structural mechanics refers to the modification or generalization of classical continuum theories to handle singularities, microstructures, and localization effects more effectively. It is particularly useful in scenarios where classical continuum theories (such as Cauchy elasticity) fail due to non-convexity, material instabilities, or the presence of microstructures (e.g., fractures, phase transitions, and strain localization). The main concept in relaxed continuum modeling is regularization of singularities i.e classical continuum models struggle with discontinuities (e.g., fractures, shear bands). Relaxed models introduce higher-order gradients or alternative formulations to avoid non-physical singularities. Another concept which deals with microstructure and non-convex energy functions i.e materials with microstructures (e.g., composites, foams, and biological tissues) can develop highly oscillatory strain fields.

Relaxation techniques replace the original non-convex strain energy function with a well-posed quasiconvex or rank-one convex approximation. Strain localization and softening is also the key concept of modeling in which traditional models predict unbounded strain localization, leading to mesh dependence in numerical simulations. Relaxation introduces nonlocal terms or regularization techniques (e.g., gradient damage models) to address these issues.

## 3.1 A Relaxed Version of the Cosserat Continuum Model Applied to Granular Materials

Assume the displacement field of the material point is denoted by $u$ and the microrotation of the continuum particle is assumed to be denoted by the symbol $\phi$. Further, denote the matrix of rotation by $\Phi$, which are orthogonal symmetric transformations such that $\varphi = axial(\Phi)$. Let the structural domain $\Omega$, is bounded by the boundary $\partial\Omega$. Consider now the force of external contribution to the system is represented by $\ell$, which is function of both the displacement field $u$ and the microrotation field variable $\varphi$, i.e. $\ell(u, \varphi)$ and is defined by

$$l(u,\varphi) = \int_{\Omega} (b \cdot u + m \cdot \varphi) dV + \int_{\partial\Omega_u} (t_u \cdot u) dS + \int_{\partial\Omega_\varphi} (t_\varphi \cdot \phi) dS, \tag{3.1}$$

where $b$ represents the body force, $m$ represents the body couple, $t_u$ represents the force of external contribution and $t_\phi$, denotes the traction moments. The problem is now to find $u$, $\varphi$ and $\phi$ such that

$$\inf_{u,\Phi,\varphi} \left\{ \int_{\Omega} W(\nabla u, \Phi, \nabla\varphi) dV - l(u,\varphi), \quad u = u_o \quad \text{at} \quad \partial\Omega_u \quad \text{and} \quad \varphi = \varphi_o \quad \text{at} \quad \partial\Omega_\varphi \right\}, \tag{3.2}$$

where

$$(u, \Phi, \varphi) \in W^{1,p}(\Omega, R^d) \times W^{1,p}(\Omega, so(d) \times W^{1,p}(\Omega, R^d)).$$

Above, the space $W^{1,p}$ is the Sobolev space that is the space of admissible deformations with $p \in (1, \infty)$ as the growth of the energy function $W$. Now, in the framework of generalized elasticity theory [37] the potential function $W$ in (3.2) takes the following form

$$W(\nabla u, \nabla\varphi, \Phi) = \frac{1}{2}\kappa : \bar{\mathbb{C}} : \kappa + \frac{1}{2} e : \mathbb{C} : e + \alpha(||\kappa||^2 - \beta^2 ||\text{dev}\varepsilon||^2)^2. \tag{3.3}$$

This interaction potential arises certainly because of the counter rotations of the granular particles at the microscale. The symbols $\alpha$ and $\beta$ in the interaction potential function are the non-negative constants. It is now possible to define the

macroscopic deformation tensor as

$$e = \nabla u - \Phi$$

and the rotational strain tensor as

$$\kappa = \nabla \varphi.$$

The constitutive response of the considered hyperelastic material is now computed where the the constitutive tensors of order four are defined as follows

$$\mathbb{C}(\nabla\varphi, \nabla u) = \frac{\partial^2 W(\nabla\varphi, \Phi, \nabla u)}{\partial \nabla u \otimes \partial \nabla u}$$

and

$$\bar{\mathbb{C}}(\nabla\varphi, \nabla u) = \frac{\partial^2 W(\nabla\varphi, \Phi, \nabla u)}{\partial \nabla\varphi \otimes \partial \nabla\varphi}.$$

The strain energy function in (3.3) becomes

$$W(\nabla u, \Phi, \nabla\varphi) = \left(\frac{\lambda}{2} + \frac{\lambda}{2}\right)(\mathrm{tr}\varepsilon)^2 + \mu||\mathrm{dev}\varepsilon||^2 + \mu_c||\mathrm{asy}\nabla u - \Phi||^2 + \frac{\bar{\lambda}}{2}(\mathrm{tr}\kappa)^2 + \bar{\mu}||\mathrm{sym}\kappa||^2 + \bar{\mu}_c||\mathrm{asy}\kappa||^2 + \alpha\left(||\kappa||^2 - \beta^2||\mathrm{dev}\varepsilon||^2\right)^2 \quad (3.4)$$

where $\lambda$ denotes the dilatancy constant, $\mu_c$ represents the shear modulus of the Cosserat material, $\mu$ denotes the shear modulus of elasticity, $\bar{\lambda}$ is the dilatancy constant related to Cosserat elasticity, $\varepsilon$ is the classical strain tensor, $\bar{\mu}$ represents the bending modulus, $\bar{\mu}_c$ refers to the coupled shear modulus and $\kappa$ is the Cosserat strain tensor.

The strain energy function in equation (3.4) is non-quasiconvex, which results in the minimizers not being attained in the energy minimization problem (3.2). The failure to attain these minimizers is primarily due to potential oscillations in the microrotation and displacement variables at the fine scales.

## 3.2 Energy in a Relaxed Configuration

The relaxed energy associated with the strain energy function in (3.4) is categorized into three different material regimes defined as follows:

The material point of the continuum body is said to be in phase 1, if the following holds.

$$||\kappa||^2 \geq \beta^2||\text{dev}\varepsilon||^2 + \frac{\mu}{2\alpha\beta^2}$$

The material point of the continuum body is said to be in phase 2, if the following holds.

$$\frac{\mu}{2\alpha\beta^2} \geq ||\kappa||^2 - \beta^2||\text{dev}\varepsilon||^2 \geq \frac{-\mu_o}{2\alpha}$$

The material point of the continuum body is said to be in phase 3, if the following holds.

$$\beta^2||\text{dev}\,\varepsilon||^2 - \frac{\mu_o}{2\alpha} \geq ||\kappa||^2.$$

In phase 1, of the material it is characterized by a microstructure involving micro-rotations of the continuum particles. In phase 2, of the particles, the material region is the regime where the material lacks any internal structure. In phase 3, the particles are within the material regime where there is a microstructure associated with the translations of the particles. The relaxed energy can therefore be expressed as follows

$$W^{rel} = \begin{cases} W_1^{rel}, & \text{if} \quad ||\kappa||^2 \geq \beta^2||\text{dev}\,\varepsilon||^2 + \dfrac{\mu}{2\alpha\beta^2}, \\ W_2^{rel}, & \text{if} \quad \dfrac{-\mu_o}{2\alpha} \leq ||\kappa||^2 - \beta^2||\text{dev}\,\varepsilon||^2 \leq \dfrac{\mu}{2\alpha\beta^2}, \\ W_3^{rel}, & \text{if} \quad ||\kappa||^2 \leq \beta^2||\text{dev}\,\varepsilon||^2 - \dfrac{\mu_o}{2\alpha}. \end{cases} \tag{3.5}$$

here $W^{rel}$ is the relaxed energy and $W_1^{rel}$, $W_2^{rel}$, $W_3^{rel}$ are explicitly given as

$$W_1^{rel} = \begin{cases} \begin{cases} \left(\frac{\lambda}{2}+\frac{\mu}{2}\right)(\mathrm{tr}\varepsilon)^2 + \mu_c||\mathrm{asy}\nabla u - \mathbf{E}\cdot\varphi||^2 - \frac{\mu^2}{4\alpha\beta^4} \\ +\frac{\bar{\lambda}}{2}(\mathrm{tr}\kappa)^2 + (\bar{\mu}-\bar{\mu}_c)||\mathrm{sym}\kappa||^2 + \left(\mu_o + \frac{\mu}{\beta^2}\right)||\kappa||^2 \end{cases} & \text{if} \quad \bar{\mu} < \bar{\mu}_c, \\ \begin{cases} \left(\frac{\lambda}{2}+\frac{\mu}{2}\right)(\mathrm{tr}\varepsilon)^2 + \mu_c||\mathrm{asy}\nabla u - \mathbf{E}\cdot\varphi||^2 - \frac{\mu^2}{4\alpha\beta^4} \\ +\frac{\bar{\lambda}}{2}(\mathrm{tr}\kappa)^2 + (\bar{\mu}-\bar{\mu}_c)||\mathrm{sym}\kappa||^2 + \left(\mu_o + \frac{\mu}{\beta^2}\right)||\kappa||^2 \end{cases} & \text{if} \quad \bar{\mu} \geq \bar{\mu}_c, \end{cases} \tag{3.6}$$

$$W_2^{rel} = \begin{cases} \left(\frac{\lambda}{2}+\frac{\mu}{2}\right)(\mathrm{tr}\varepsilon)^2 + \mu_c||\mathrm{asy}\nabla u - \mathbf{E}\cdot\varphi||^2 + \mu||\mathrm{dev}\,\varepsilon||^2 + \frac{\bar{\lambda}}{2}(\mathrm{tr}\kappa)^2 \\ +\bar{\mu}||\mathrm{sym}\kappa||^2 + \bar{\mu}_c||\mathbf{asy}\kappa||^2 + \alpha\left(||\mathbf{sym}\kappa||^2 + ||\mathrm{asy}\kappa||^2 - \beta^2||\mathrm{dev}\,\varepsilon||^2\right)^2 \end{cases}, \tag{3.7}$$

and

$$W_3^{rel} = \begin{cases} \begin{cases} \left(\frac{\lambda}{2}+\frac{\mu}{2}\right)(\mathrm{tr}\varepsilon)^2 + \mu_c||\mathrm{asy}\nabla u - \mathbf{E}\cdot\varphi||^2 - \frac{\mu^2}{4\alpha} \\ +\frac{\bar{\lambda}}{2}(\mathrm{tr}\kappa)^2 + (\bar{\mu}-\bar{\mu}_c)||\mathrm{sym}\kappa||^2 + \left(\mu_o + \frac{\mu}{\beta^2}\right)||\mathrm{dev}\,\varepsilon||^2 \end{cases} & \text{if} \quad \bar{\mu} < \bar{\mu}_c, \\ \begin{cases} \left(\frac{\lambda}{2}+\frac{\mu}{2}\right)(\mathrm{tr}\varepsilon)^2 + \mu_c||\mathrm{asy}\nabla u - \mathbf{E}\cdot\varphi||^2 - \frac{\mu^2}{4\alpha} \\ +\frac{\bar{\lambda}}{2}(\mathrm{tr}\kappa)^2 + (\bar{\mu}-\bar{\mu}_c)||\mathrm{sym}\kappa||^2 + \left(\mu_o + \frac{\mu}{\beta^2}\right)||\mathrm{dev}\,\varepsilon||^2 \end{cases} & \text{if} \quad \bar{\mu} \geq \bar{\mu}_c. \end{cases} \tag{3.8}$$

respectively. Now calculating the analytical form of the relaxed strain energy related to the non-quasi-convex strain energy potential in (3.4) makes it possible to expect any microstructure of the material and to shift the respective computational task from the material or microscopic scale to the component or macroscopic one.

As a result, important details about the evolution of microstructure in the granular materials become possible which is essential in determining their gross mechanical response. For practical purposes, as the current stage of techniques development

use this relaxed potential, much effort is not required to reformulate the non-quasi-convex energy minimization problem in (3.2) as a finding minimization of relaxed strain energy.

## 3.3 A Two-field Variational Approach

The fundamental aspect of the Cosserat continuum theory is the inclusion of the couple stress tensor in the momentum conservation equations which leads to the couple strain deformation within the elastic model. The variational principle in (3.2) now can be used to derive the balance equations governing the material response.

Let us take the variations of equation (3.2) in the displacement $u$ and the micro-rotation field variable $\phi$, we obtain the following PDEs representing the balance of linear and angular momentum,

$$\nabla \cdot \sigma = \mathbf{b}, \tag{3.9}$$

$$\nabla \cdot \mu + \sigma : \mathbf{E} = \mathbf{m}. \tag{3.10}$$

Here, the symbol $\mathbf{E}$ represents the third order tensor known as permutation tensor, the vector $\mathbf{b}$ denotes the body force vector and $\mathbf{m}$ represents moment force vector. The problem is defined by prescribing certian boundary conditions of the Drichlet and Neumann type respectively as follows

$$t_u = \sigma \cdot N_u,$$

and

$$t_\phi = \mu \cdot N_\phi.$$

The constitutive response of the material is now calculated using the following relations

$$\boldsymbol{\sigma} = \frac{\partial W^{rel}}{\partial e}, \tag{3.11}$$

$$\boldsymbol{\mu} = \frac{\partial W^{rel}}{\partial \kappa}, \tag{3.12}$$

where $\boldsymbol{\sigma}$ represents the Cauchy stress tensor and $\boldsymbol{\mu}$ represents the Cosserat stress tensor. Now, in order to derive the weak formulation of the problem in (3.9), we select arbitrary variations in the displacement and microrotation fields, denoted as $\delta u, \delta\varphi$, respectively.

The weak formulation is

$$\int_{\Omega} b \cdot \delta u \, d\Omega + \int_{\Gamma_u} t_u \cdot \delta u \, d\Gamma_u = \int_{\Omega} \sigma : (\nabla \otimes \delta u) d\Omega, \tag{3.13}$$

and

$$\int_{\Omega} m \cdot \delta\phi \, d\Omega + \int_{\Gamma_\varphi} t_\varphi \cdot \delta\phi \, d\Gamma_\phi = \int_{\Omega} \mu : \nabla \otimes \delta\phi \, d\Omega - \int_{\Omega} \sigma : \mathbf{E}) \cdot \delta\phi \, d\Omega, \tag{3.14}$$

where, $t_u = \sigma \cdot N_u$ is traction applied on the boundary $\Gamma_u$, $N_u$ being the normal unit vector to $\Gamma_u$, $t_u$ and $t_\phi$ be the traction and moment forces on $\Gamma_u$ and $\Gamma_\phi$, respectively, and $n_u$ and $n_\phi$ are the normal unit vectors.

Note that in calculating the above equations (3.13) and (3.14) the divergence theorem is applied with the following properties

$$\nabla \cdot (\mu \cdot \delta\varphi) = \nabla \cdot (\mu) \cdot \delta\varphi + \mu : (\nabla \otimes \delta\phi),$$

and

$$\mathbf{E} : \sigma = \sigma : \mathbf{E}.$$

The weak governing equations in (3.9) and (3.10) must be satisfied for the equilibrium configuration of a body at each material point in a Cosserat continuum. There are many similarities between the finite volume method and the finite element method. In **2D**, the domain consists of a set of discrete finite elements, which are usually triangles or quadrilaterals; in **3D**, tetrahedra or hexahedra are more frequently utilized.

Before integrating the equations over the entire domain, they are multiplied by a weight function. To maintain continuity of the solution across element boundaries,

the simplest finite element methods use a linear shape function to approximate the solution within each element. This function can be constructed from the values at the corners of the elements. Typically, the weight function takes the similar shape. By substituting this approximation into the weighted integral of the conservation law, the equations that need to be solved are derived by setting that the derivative of the integral with respect to each nodal value is zero. This indicates that the best solution within the set of allowed functions should be chosen (the one with the least residual). A collection of non-linear algebraic equations is the end product. Moreover, a brief discussion has been done for the numerical methodology adopted for the solution of governing equations.

# Chapter 4

# Finite Element Setting and Numerical Implementation of Model Problem

## 4.1 Numerical Calculations of Cosserat Elasticity Model

The weak form of the balance equations in (3.13) and (3.14) are solved numerically through the application of finite element procedure. Here we have assumed that the working problem is in the absence of body force and body couple. The material domain $\Omega$ is discretized as follows

$$\Omega = \bigcup_{e=1}^{n_e} \Omega^e, \qquad \Omega^p \cap \Omega^q = \emptyset \quad \text{for} \quad p \neq q$$

where $n_e$ represents number of triangular elements in the computational domain $\Omega$. It is easy to etablish a local coordinate system $(\xi_1, \xi_2, \xi_3)$ for each element $\Omega^e$ such that $-1 \leq \xi_1 \leq 1, -1 \leq \xi_2 \leq 1$ and $-1 \leq \xi_3 \leq 1$. The field variables within $\Omega^e$ can be interpolated using the nodal shape functions defined in this local coordinate

system. In the framework of Cosserat continuum these field variables include displacement and micro-rotation, which together contains a total number of nine degrees of freedom at a single material point within an element $\Omega^e$. The three displacement components $\{u_p^e; p = 1, 2, 3\}$ and three microrotation components $\{\varphi_p^e; p = 1, 2, 3\}$ are approximated at the nodes of each triangular element $\Omega^e$ using test functions as follows

$$u_p^e \approx \sum_{m=1}^{N} N^m(\xi_1, \xi_2, \xi_3)\bar{u}_p^e$$

and

$$\varphi_p^e \approx \sum_{m=1}^{N} N^m(\xi_1, \xi_2, \xi_3)\bar{\varphi}_p^e, \quad ; p = 1, 2, 3.$$

$\{N^m(\xi_1, \xi_2, \xi_3)\}_{m=1}^N$ are the shape/test functions at each node of the triangular element $\Omega_e$.

The strains at each triangular element $\Omega^e$ is then approximated using the following definitions

$$e_{pq}^e = u_{q,p}^e - E_{pqr}\varphi_r^e, \tag{4.1}$$

$$\kappa_{pq}^e = \varphi_{q,p}^e, \tag{4.2}$$

herein $E_{pqr}$ indicates the cartesian permutations, takes zero value if any of the indices p, q and r is repeating, takes 1 if p, q and r is a cyclic permutation and -1 otherwise, whereas

$$u_{q,p}^e \approx \sum_{m}^{N}\sum_{n}^{3} \frac{\partial N^m}{\partial \xi_n}\frac{\partial \xi_n}{\partial X_p}\tilde{u}_q^e, \tag{4.3}$$

$$\varphi_{q,p}^e \approx \sum_{m}^{N}\sum_{n}^{3} \frac{\partial N^m}{\partial \xi_n}\frac{\partial \xi_n}{\partial X_p}\tilde{\varphi}_q^e. \tag{4.4}$$

In each direction, let $X_p$ represent the physical coordinate. These quantities can be expressed in vector notation as

$$\sigma^e = [\sigma_{11}^e, \sigma_{22}^e, \sigma_{33}^e, \sigma_{12}^e, \sigma_{21}^e, \sigma_{13}^e, \sigma_{31}^e, \sigma_{23}^e, \sigma_{32}^e]^T, \tag{4.5}$$

$$\mu^e = [\mu_{11}^e, \mu_{22}^e, \mu_{33}^e, \mu_{12}^e, \mu_{21}^e, \mu_{13}^e, \mu_{31}^e, \mu_{23}^e, \mu_{32}^e]^T, \tag{4.6}$$

where $\sigma^e_{pq}$ and $\mu^e_{pq}$ in each material regime are calculated with the following formulae.

In the material regime with phase 1 these stresses are computed as

$$\sigma^e_{pq} = 2\left(\frac{\lambda}{2} + \frac{\mu}{d}\right)\varepsilon^e_{rr}\delta_{pq} + \mu_c(u^e_{q,p} - u^e_{p,q}) - 2\mu_c E_{pqr}\varphi^e_r, \tag{4.7}$$

$$\mu^e_{pq} = \begin{cases} \bar{\lambda}\kappa^e_{rr}\delta_{pq} + (\bar{\mu} - \bar{\mu}_c)(\kappa^e_{pq} + \kappa^e_{qp}) + 2\left(\mu_o + \frac{\mu}{\beta^2}\right)\kappa^e_{pq} & \text{if} \quad \bar{\mu} \geq \bar{\mu}_c, \\ \bar{\lambda}\kappa^e_{rr}\delta_{pq} - (\bar{\mu} - \bar{\mu}_c)(\kappa^e_{pq} - \kappa^e_{qp}) + 2\left(\mu_o + \frac{\mu}{\beta^2}\right)\kappa^e_{pq} & \text{if} \quad \bar{\mu} < \bar{\mu}_c. \end{cases} \tag{4.8}$$

In the material regime denoted with phase 2 these stresses are computed as

$$\sigma^e_{pq} = \begin{cases} \bar{\lambda}\varepsilon^e_{rr}\delta pq + (\mu + \mu_c)u^e_{q,p}(\mu - \mu_c)u^e_{p,q} - 2\mu_c E_{pqr}\varphi^e_r, \\ -4\alpha\beta^2\left((\kappa^e_{pq})^2 - \beta^2(\varepsilon^e_{pq} - \frac{1}{d}\varepsilon^e_{rr}\delta_{pq})^2\right)\left(\varepsilon^e_{pq} - \frac{1}{d}\varepsilon^e_{rr}\delta_{pq}\right). \end{cases} \tag{4.9}$$

$$\begin{aligned} \mu^e_{pq} = \bar{\lambda}\kappa^e_{rr}\delta_{pq} + (\bar{\mu} + \bar{\mu}_c)\kappa^e_{pq} + (\bar{\mu} - \bar{\mu}_c)\kappa^e_{qp} \\ + 4\alpha\left((\kappa^e_{pq})^2 - \beta^2(\varepsilon^e_{pq} - \frac{1}{d}\varepsilon^e_{rr}\delta_{pq})^2\right)\kappa^e_{pq}, \end{aligned} \tag{4.10}$$

In the material regime denoted with phase 3 these stresses are computed as

$$\begin{aligned} \sigma^e_{pq} = \bar{\lambda}\varepsilon^e_{rr}\delta pq + (\mu + \mu_c)u^e_{q,p} + (\mu - \mu_c)u^e_{p,q} - 2\mu_c E_{pqr}\varphi^e_r \\ + 2\mu_o\beta^2\left(\varepsilon^e_{pq} - -\frac{1}{d}\varepsilon^e_{rr}\delta_{pq}\right), \end{aligned} \tag{4.11}$$

$$\mu^e_{pq} = \begin{cases} \bar{\lambda}\kappa^e_{rr}\delta_{pq} + (\bar{\mu} - \bar{\mu}_c)(\kappa^e_{pq} + \kappa^e_{qp}) & \text{if} \quad \bar{\mu} \geq \bar{\mu}_c, \\ \bar{\lambda}\kappa^e_{rr}\delta_{pq} - (\bar{\mu} - \bar{\mu}_c)(\kappa^e_{pq} - \kappa^e_{qp}) & \text{if} \quad \bar{\mu} < \bar{\mu}_c. \end{cases} \tag{4.12}$$

Here in the Cosserat theory, we are considering couple of stresses in elastic continuum.

Hence, to acquire the balance of forces and moments with b=0 and m=0, i.e.

$$\nabla \cdot \sigma = 0, \tag{4.13}$$

$$\nabla \cdot \mu + \text{asy}\sigma = 0, \tag{4.14}$$

and considering rotation only in third direction with $v_1, v_2$ and $\tilde{w}_3$ are the test functions.

Hence, variational formulation of (4.13) and (4.14) will be respectively, as

$$\int_{\Omega} (\sigma_{11} v_{1,1} + \sigma_{12} v_{2,1} + \sigma_{21} v_{1,2} + \sigma_{22} v_{2,2})\, d\Omega - \int_{\Gamma_u} (t_1 v_1 + t_2 v_2)\, d\Gamma_u = 0, \tag{4.15}$$

$$\int_{\Omega} (\mu_{13} \tilde{w}_{3,1} + \mu_{23} \tilde{w}_{3,2} - (\sigma_{12} - \sigma_{21}) \tilde{w}_3\, d\Omega - \int_{\Gamma_\phi} (t_1 w_1 + t_2 w_2)\, d\Gamma_\phi = 0. \tag{4.16}$$

where for a nonlinear constitutive relations in a cosserat medium, $\sigma$ is

$$\sigma = \begin{cases} \dfrac{\partial W_1^{rel}}{\partial \nabla u}, & \text{if} \quad ||\nabla \phi||^2 \geq \beta^2 ||\text{dev sym} \nabla u||^2 + \dfrac{\mu}{2\alpha\beta^2}, \\ \dfrac{\partial W_2^{rel}}{\partial \nabla u}, & \text{if} \quad \dfrac{-\mu_o}{2\alpha} \leq ||\nabla \phi||^2 - \beta^2 ||\text{dev sym} \nabla u||^2 \leq \dfrac{\mu}{2\alpha\beta^2}, \\ \dfrac{\partial W_3^{rel}}{\partial \nabla u}, & \text{if} \quad ||\nabla \phi||^2 \leq \beta^2 ||\text{dev sym} \nabla u||^2 - \dfrac{\mu_o}{2\alpha}. \end{cases} \tag{4.17}$$

where $\boldsymbol{W} = (W_1, W_2.W_3)$ are the components of relaxed energies and hence,

$$\frac{\partial W_1^{rel}}{\partial \nabla u} = \left(\frac{\lambda}{2} + \frac{\mu}{d}\right) (\text{tr}(\nabla u + \nabla u^T))\boldsymbol{I} + \mu_c((\nabla u - \nabla u^T) - 2\epsilon \cdot \phi), \tag{4.18}$$

$$\begin{aligned} \frac{\partial W_2^{rel}}{\partial \nabla u} = \frac{\lambda}{2}(\text{tr}(\nabla u + \nabla u^T)\boldsymbol{I} + \mu((\nabla u + \nabla u^T)) + \mu_c((\nabla u - \nabla u^T) - 2\epsilon \cdot \phi) \\ - 4\alpha\beta^2 \left(||\nabla \phi||^2 - \beta^2 ||\text{dev sym} \nabla u||^2\right) (\text{dev sym} \nabla u), \end{aligned} \tag{4.19}$$

and

$$\begin{aligned} \frac{\partial W_3^{rel}}{\partial \nabla u} = \frac{\lambda}{2}(\text{tr}(\nabla u + \nabla u^T)\boldsymbol{I} + \mu(\nabla u + \nabla u^T) + 2\mu_o\beta^2(dev(\nabla u + \nabla u^T)) \\ + \mu_c((\nabla u - \nabla u^T) - 2\epsilon \cdot \phi), \end{aligned} \tag{4.20}$$

In components form, we have

$$\bar{\boldsymbol{u}}^e = (u_1, u_2, 0) \quad \text{and} \quad \phi = (0, 0, \phi_3)$$

and

$$\mathrm{sym}\nabla u = \begin{bmatrix} \dfrac{\partial u}{\partial x} & \dfrac{1}{2}(\dfrac{\partial u}{\partial y} + \dfrac{\partial v}{\partial x}) \\ \dfrac{1}{2}(\dfrac{\partial u}{\partial y} + \dfrac{\partial v}{\partial x}) & \dfrac{\partial v}{\partial y} \end{bmatrix},$$

$$\mathrm{asy}\nabla u = \begin{bmatrix} 0 & \dfrac{1}{2}(\dfrac{\partial u}{\partial y} - \dfrac{\partial v}{\partial x}) \\ \dfrac{1}{2}(\dfrac{\partial v}{\partial x} - \dfrac{\partial u}{\partial y}) & 0 \end{bmatrix},$$

$$\nabla\phi = \begin{bmatrix} \dfrac{\partial\phi_1}{\partial x} & \dfrac{\partial\phi_1}{\partial y} & \dfrac{\partial\phi_1}{\partial z} \\ \dfrac{\partial\phi_2}{\partial x} & \dfrac{\partial\phi_2}{\partial y} & \dfrac{\partial\phi_2}{\partial z} \\ \dfrac{\partial\phi_3}{\partial x} & \dfrac{\partial\phi_3}{\partial y} & \dfrac{\partial\phi_3}{\partial z} \end{bmatrix}.$$

As rotation is only in third direction thus, we have

$$\nabla\phi = \begin{bmatrix} 0 & 0 & 0 \\ 0 & 0 & 0 \\ \dfrac{\partial\phi_3}{\partial x} & \dfrac{\partial\phi_3}{\partial y} & 0 \end{bmatrix},$$

$$\mathrm{sym}\nabla\phi = \begin{bmatrix} \dfrac{\partial\phi_1}{\partial x} & \dfrac{1}{2}\left(\dfrac{\partial\phi_1}{\partial y} + \dfrac{\partial\phi_2}{\partial x}\right) & \dfrac{1}{2}\left(\dfrac{\partial\phi_1}{\partial z} + \dfrac{\partial\phi_3}{\partial x}\right) \\ \dfrac{1}{2}\left(\dfrac{\partial\phi_1}{\partial y} + \dfrac{\partial\phi_2}{\partial x}\right) & \dfrac{\partial\phi_2}{\partial y} & \dfrac{1}{2}\left(\dfrac{\partial\phi_2}{\partial z} + \dfrac{\partial\phi_3}{\partial y}\right) \\ \dfrac{1}{2}\left(\dfrac{\partial\phi_1}{\partial z} + \dfrac{\partial\phi_3}{\partial x}\right) & \dfrac{1}{2}\left(\dfrac{\partial\phi_2}{\partial z} + \dfrac{\partial\phi_3}{\partial y}\right) & \dfrac{\partial\phi_3}{\partial z} \end{bmatrix},$$

$$\mathrm{asy}\nabla\phi = \begin{bmatrix} 0 & \dfrac{1}{2}\left(\dfrac{\partial\phi_1}{\partial y} - \dfrac{\partial\phi_2}{\partial x}\right) & \dfrac{1}{2}\left(\dfrac{\partial\phi_1}{\partial z} - \dfrac{\partial\phi_3}{\partial x}\right) \\ \dfrac{1}{2}\left(\dfrac{\partial\phi_2}{\partial x} - \dfrac{\partial\phi_1}{\partial y}\right) & 0 & \dfrac{1}{2}\left(\dfrac{\partial\phi_2}{\partial z} - \dfrac{\partial\phi_3}{\partial y}\right) \\ \dfrac{1}{2}\left(\dfrac{\partial\phi_3}{\partial x} - \dfrac{\partial\phi_1}{\partial z}\right) & \dfrac{1}{2}\left(\dfrac{\partial\phi_3}{\partial y} - \dfrac{\partial\phi_2}{\partial z}\right) & 0 \end{bmatrix},$$

$$\epsilon\cdot\phi = \begin{bmatrix} 0 & \epsilon_{123}\phi_3 \\ \epsilon_{213}\phi_3 & 0 \end{bmatrix},$$

$$\epsilon \cdot \phi = \begin{bmatrix} 0 & \phi_3 \\ -\phi_3 & 0 \end{bmatrix},$$

$$\text{dev sym}\nabla u = \begin{bmatrix} \frac{1}{2}\left(\frac{\partial u}{\partial x} - \frac{\partial v}{\partial y}\right) & \frac{1}{2}\left(\frac{\partial u}{\partial y} + \frac{\partial v}{\partial x}\right) \\ \frac{1}{2}\left(\frac{\partial u}{\partial y} + \frac{\partial v}{\partial x}\right) & \frac{1}{2}\left(\frac{\partial v}{\partial y} - \frac{\partial u}{\partial x}\right) \end{bmatrix},$$

$$||\text{dev sym}\nabla u||^2 = \frac{1}{4}\left(\frac{\partial u}{\partial x} - \frac{\partial v}{\partial y}\right)^2 + \frac{1}{4}\left(\frac{\partial u}{\partial y} + \frac{\partial v}{\partial x}\right)^2 + \frac{1}{4}\left(\frac{\partial u}{\partial y} + \frac{\partial v}{\partial x}\right)^2 + \frac{1}{4}\left(\frac{\partial v}{\partial y} - \frac{\partial u}{\partial x}\right)^2,$$

and

$$||\nabla \phi||^2 = \left(\frac{\partial \phi_3}{\partial x}\right)^2 + \left(\frac{\partial \phi_3}{\partial y}\right)^2.$$

By putting all these values in (4.18), we get

$$\frac{\partial W_1^{rel}}{\partial \nabla u} = 2\left(\frac{\lambda}{2} + \frac{\mu}{d}\right)\left(\frac{\partial u}{\partial x} + \frac{\partial v}{\partial y}\right)\begin{bmatrix} 1 & 0 \\ 0 & 1 \end{bmatrix} + 2\mu_c\left(\begin{bmatrix} 0 & \frac{1}{2}\left(\frac{\partial u}{\partial y} - \frac{\partial v}{\partial x}\right) \\ \frac{1}{2}\left(\frac{\partial v}{\partial x} - \frac{\partial u}{\partial y}\right) & 0 \end{bmatrix} - \begin{bmatrix} 0 & \epsilon_{123}\phi_3 \\ \epsilon_{213}\phi_3 & 0 \end{bmatrix}\right), \quad (4.21)$$

$$\frac{\partial W_1^{rel}}{\partial \nabla u} = \left(\lambda\frac{\partial u}{\partial x} + \lambda\frac{\partial v}{\partial y} + \frac{2\mu_c}{d}\frac{\partial u}{\partial x} + \frac{2\mu}{d}\frac{\partial v}{\partial y}\right)\begin{bmatrix} 1 & 0 \\ 0 & 1 \end{bmatrix} + \begin{bmatrix} 0 & \mu_c\left(\left(\frac{\partial u}{\partial y} - \frac{\partial v}{\partial x}\right) - 2\epsilon_{123}\phi_3\right) \\ \mu_c\left(\left(\frac{\partial v}{\partial x} - \frac{\partial u}{\partial y}\right) - 2\epsilon_{213}\phi_3\right) & 0 \end{bmatrix},$$

$$\frac{\partial W_1^{rel}}{\partial \nabla u} = \begin{bmatrix} \left(\lambda\frac{\partial u}{\partial x} + \lambda\frac{\partial v}{\partial y} + \frac{2\mu}{d}\frac{\partial u}{\partial x} + \frac{2\mu}{d}\frac{\partial v}{\partial y}\right) & \mu_c\left(\left(\frac{\partial u}{\partial y} - \frac{\partial v}{\partial x}\right) - 2\epsilon_{123}\phi_3\right) \\ \mu_c\left(\left(\frac{\partial v}{\partial x} - \frac{\partial u}{\partial y}\right) - 2\epsilon_{213}\phi_3\right) & \left(\lambda\frac{\partial u}{\partial x} + \lambda\frac{\partial v}{\partial y} + \frac{2\mu}{d}\frac{\partial u}{\partial x} + \frac{2\mu}{d}\frac{\partial v}{\partial y}\right) \end{bmatrix},$$

or

$$\frac{\partial W_1^{rel}}{\partial \nabla u} = \begin{bmatrix} \left(\lambda + \frac{2\mu}{d}\right)\left(\frac{\partial u}{\partial x} + \frac{\partial v}{\partial y}\right) & \mu_c\left(\left(\frac{\partial u}{\partial y} - \frac{\partial v}{\partial x}\right) - 2\phi_3\right) \\ \mu_c\left(\left(\frac{\partial v}{\partial x} - \frac{\partial u}{\partial y}\right) + 2\phi_3\right) & \left(\lambda + \frac{2\mu}{d}\right)\left(\frac{\partial u}{\partial x} + \frac{\partial v}{\partial y}\right) \end{bmatrix}. \tag{4.22}$$

$$\begin{aligned} \frac{\partial W_2^{rel}}{\partial \nabla u} = & \begin{bmatrix} (\lambda + 2\mu)\frac{\partial u}{\partial x} + \lambda\frac{\partial v}{\partial y} & B_{11} - 2\mu_c\phi_3 \\ B_{12} + 2\mu_c\phi_3 & (\lambda + 2\mu)\frac{\partial v}{\partial y} + \lambda\frac{\partial u}{\partial x} \end{bmatrix} \\ & - 4\alpha\beta^2\left[\left(\frac{\partial \phi_3}{\partial x}\right)^2 + \left(\frac{\partial \phi_3}{\partial y}\right)^2 - \frac{\beta^2}{4}\left(\frac{\partial u}{\partial x} - \frac{\partial v}{\partial y}\right)^2\right. \\ & \left. - \frac{\beta^2}{4}\left(\frac{\partial u}{\partial y} + \frac{\partial v}{\partial x}\right)^2 - \frac{\beta^2}{4}\left(\frac{\partial v}{\partial y} - \frac{\partial u}{\partial x}\right)^2 - \frac{\beta^2}{4}\left(\frac{\partial u}{\partial y} + \frac{\partial v}{\partial x}\right)^2\right] \\ & \begin{bmatrix} \frac{1}{2}\left(\frac{\partial u}{\partial x} - \frac{\partial v}{\partial y}\right) & \frac{1}{2}\left(\frac{\partial u}{\partial y} + \frac{\partial v}{\partial x}\right) \\ \frac{1}{2}\left(\frac{\partial u}{\partial y} + \frac{\partial v}{\partial x}\right) & \frac{1}{2}\left(\frac{\partial v}{\partial y} - \frac{\partial u}{\partial x}\right) \end{bmatrix}, \end{aligned} \tag{4.23}$$

where

$$B_{11} = (\mu_c + \mu)\frac{\partial u}{\partial y} + (\mu - \mu_c)\frac{\partial v}{\partial x},$$

$$B_{12} = (\mu_c + \mu)\frac{\partial v}{\partial x} + (\mu - \mu_c)\frac{\partial u}{\partial y},$$

and

$$\frac{\partial W_3^{rel}}{\partial \nabla u} = \begin{bmatrix} M_{11}u_x + M_{12}u_y & M_{21}u_y + M_{22}v_x - 2\mu_c\phi_3 \\ M_{21}v_x + M_{22}u_y + 2\mu_c\phi_3 & M_{11}v_y + M_{12}u_x \end{bmatrix}. \tag{4.24}$$

where

$$M_{11} = \left(\lambda + 2\mu + \mu_o\beta^2\right),$$

$$M_{12} = (\lambda - \mu_o\beta^2),$$

$$M_{21} = (\mu_c + \mu + \mu_o\beta^2),$$

and

$$M_{22} = (\mu - \mu_c + \mu_o\beta^2).$$

and now for $\mu$ we have

$$\mu = \begin{cases} \dfrac{\partial W_1^{rel}}{\partial \nabla\phi}, & \text{if} \quad ||\nabla\phi||^2 \geq \beta^2 ||\text{dev sym}\nabla u||^2 + \dfrac{\mu}{2\alpha\beta^2}, \\ \dfrac{\partial W_2^{rel}}{\partial \nabla\phi}, & \text{if} \quad \dfrac{-\mu_o}{2\alpha} \leq ||\nabla\phi||^2 - \beta^2 ||\text{dev sym}\nabla u||^2 \leq \dfrac{\mu}{2\alpha\beta^2}, \\ \dfrac{\partial W_3^{rel}}{\partial \nabla\phi}, & \text{if} \quad ||\nabla\phi||^2 \leq \beta^2 ||\text{dev sym}\nabla u||^2 - \dfrac{\mu_o}{2\alpha}. \end{cases} \tag{4.25}$$

Let $c' = (\bar{\mu} - \bar{\mu}_c)$. Thus we have

$$\frac{\partial W_1^{rel}}{\partial \nabla\phi} = \begin{cases} 2\left(\mu_o + \frac{\mu}{\beta^2}\right) \begin{bmatrix} 0 & 0 & 0 \\ 0 & 0 & 0 \\ \dfrac{\partial\phi_3}{\partial x} & \dfrac{\partial\phi_3}{\partial y} & 0 \end{bmatrix} + c' \begin{bmatrix} 0 & 0 & \dfrac{\partial\phi_3}{\partial x} \\ 0 & 0 & \dfrac{\partial\phi_3}{\partial y} \\ \dfrac{\partial\phi_3}{\partial x} & \dfrac{\partial\phi_3}{\partial y} & 0 \end{bmatrix}, & \text{if} \quad \bar{\mu} \geq \bar{\mu}_c \\ 2\left(\mu_o + \frac{\mu}{\beta^2}\right) \begin{bmatrix} 0 & 0 & 0 \\ 0 & 0 & 0 \\ \dfrac{\partial\phi_3}{\partial x} & \dfrac{\partial\phi_3}{\partial y} & 0 \end{bmatrix} - c' \begin{bmatrix} 0 & 0 & \dfrac{-\partial\phi_3}{\partial x} \\ 0 & 0 & \dfrac{-\partial\phi_3}{\partial y} \\ \dfrac{\partial\phi_3}{\partial x} & \dfrac{\partial\phi_3}{\partial y} & 0 \end{bmatrix}, & \text{if} \quad \bar{\mu} \leq \bar{\mu}_c \end{cases} \tag{4.26}$$

or, we can write it as

$$\frac{\partial W_1^{rel}}{\partial \nabla\phi} = \begin{cases} \begin{bmatrix} 0 & 0 & c'\dfrac{\partial\phi_3}{\partial x} \\ 0 & 0 & c'\dfrac{\partial\phi_3}{\partial y} \\ A_{11}\dfrac{\partial\phi_3}{\partial x} & A_{11}\dfrac{\partial\phi_3}{\partial x} & 0 \end{bmatrix}, & \text{if} \quad \bar{\mu} \geq \bar{\mu}_c \\ \begin{bmatrix} 0 & 0 & c'\dfrac{\partial\phi_3}{\partial x} \\ 0 & 0 & c'\dfrac{\partial\phi_3}{\partial y} \\ A_{12}\dfrac{\partial\phi_3}{\partial x} & A_{12}\dfrac{\partial\phi_3}{\partial x} & 0 \end{bmatrix}, & \text{if} \quad \bar{\mu} \leq \bar{\mu}_c \end{cases} \tag{4.27}$$

where

$$A_{11} = \left( \bar{\mu} - \bar{\mu}_c + 2(\mu_o + \frac{\mu}{\beta^2}) \right),$$

$$A_{12} = \left( \bar{\mu}_c - \bar{\mu} + 2(\mu_o + \frac{\mu}{\beta^2}) \right).$$

$$\begin{aligned}
\frac{\partial W_2^{rel}}{\partial \nabla \phi} = \bar{\mu} & \begin{bmatrix} 0 & 0 & \dfrac{\partial \phi_3}{\partial x} \\ 0 & 0 & \dfrac{\partial \phi_3}{\partial y} \\ \dfrac{\partial \phi_3}{\partial x} & \dfrac{\partial \phi_3}{\partial y} & 0 \end{bmatrix} + \bar{\mu}_c \begin{bmatrix} 0 & 0 & \dfrac{-\partial \phi_3}{\partial x} \\ 0 & 0 & \dfrac{-\partial \phi_3}{\partial y} \\ \dfrac{\partial \phi_3}{\partial x} & \dfrac{\partial \phi_3}{\partial y} & 0 \end{bmatrix} \\
& + 4\alpha \left( \left( \frac{\partial \phi_3}{\partial x} \right)^2 + \left( \frac{\partial \phi_3}{\partial y} \right)^2 - \beta^2 \left( \frac{1}{4} \left( \frac{\partial u}{\partial x} - \frac{\partial v}{\partial y} \right)^2 + \frac{1}{4} \left( \frac{\partial u}{\partial y} + \frac{\partial v}{\partial x} \right)^2 \right) \right. \\
& \left. + \left( \frac{1}{4} \left( \frac{\partial u}{\partial y} + \frac{\partial v}{\partial x} \right)^2 + \frac{1}{4} \left( \frac{\partial v}{\partial y} - \frac{\partial u}{\partial x} \right)^2 \right) \begin{bmatrix} 0 & 0 & 0 \\ 0 & 0 & 0 \\ \dfrac{\partial \phi_3}{\partial x} & \dfrac{\partial \phi_3}{\partial y} & 0 \end{bmatrix} \right), \quad (4.28)
\end{aligned}$$

or

$$\begin{aligned}
\frac{\partial W_2^{rel}}{\partial \nabla \phi} = & \begin{bmatrix} 0 & 0 & (\bar{\mu} - \bar{\mu}_c) \left( \dfrac{\partial \phi_3}{\partial x} \right) \\ 0 & 0 & (\bar{\mu} - \bar{\mu}_c) \left( \dfrac{\partial \phi_3}{\partial y} \right) \\ (\bar{\mu} + \bar{\mu}_c) \left( \dfrac{\partial \phi_3}{\partial x} \right) & (\bar{\mu} + \bar{\mu}_c) \left( \dfrac{\partial \phi_3}{\partial y} \right) & 0 \end{bmatrix} \\
-4\alpha & \left( \beta^2 \left( \frac{1}{4} \left( \frac{\partial u}{\partial x} - \frac{\partial v}{\partial y} \right)^2 + \frac{1}{4} \left( \frac{\partial u}{\partial y} + \frac{\partial v}{\partial x} \right)^2 + \frac{1}{4} \left( \frac{\partial u}{\partial y} + \frac{\partial v}{\partial x} \right)^2 + \frac{1}{4} \left( \frac{\partial v}{\partial y} - \frac{\partial u}{\partial x} \right)^2 \right) \right. \\
& \left. + \left( \frac{\partial \phi_3}{\partial x} \right)^2 + \left( \frac{\partial \phi_3}{\partial y} \right)^2 \begin{bmatrix} 0 & 0 & 0 \\ 0 & 0 & 0 \\ \dfrac{\partial \phi_3}{\partial x} & \dfrac{\partial \phi_3}{\partial y} & 0 \end{bmatrix} \right), \quad (4.29)
\end{aligned}$$

and

$$\frac{\partial W_3^{rel}}{\partial \nabla \phi} = \begin{cases} \begin{bmatrix} 0 & 0 & c' \dfrac{\partial \phi_3}{\partial x} \\ 0 & 0 & c' \dfrac{\partial \phi_3}{\partial y} \\ (\bar{\mu} - \bar{\mu}_c) \dfrac{\partial \phi_3}{\partial x} & (\bar{\mu} - \bar{\mu}_c) \dfrac{\partial \phi_3}{\partial x} & 0 \end{bmatrix}, & \text{if} \quad \bar{\mu} \geq \bar{\mu}_c \\ \begin{bmatrix} 0 & 0 & c' \dfrac{\partial \phi_3}{\partial x} \\ 0 & 0 & c' \dfrac{\partial \phi_3}{\partial y} \\ (\bar{\mu}_c - \bar{\mu}) \dfrac{\partial \phi_3}{\partial x} & (\bar{\mu}_c - \bar{\mu}) \dfrac{\partial \phi_3}{\partial x} & 0. \end{bmatrix}. & \text{if} \quad \bar{\mu} \leq \bar{\mu}_c \end{cases} \tag{4.30}$$

Now, for further numerical simulations we used FreeFEM++.

## 4.2 Algorithm for Solving Continuum Model

**Step 1:** Initialize the parameters $\lambda, \mu, \bar{\mu}, \alpha, E, \nu, \beta, \mu, \mu_c, \mu_o$.

**Step 2:** For each time interval, dicretize into $t_{nts}$ time steps as:

$$t_{n+1} = t_n + \Delta t_{n+1}, \quad n \in \{0, 1, 2, 3, \ldots, t_{\text{nts}}\}.$$

**Step 3:** Initialize the field variables

$$u^i = 0, \quad \phi^i = 0.$$

**Step 4:** Calculate Cosserat strains $\nabla u^i$ and coupled strain $\nabla \phi^i$.

**Step 5:** Compute the term:

$$||\nabla \phi||^2 - \beta^2 ||\text{dev sym} \nabla us||^2,$$

**Step 6: In phase 1**

if $||\nabla \phi||^2 - \beta^2 ||\text{dev sym} \nabla u||^2 > \dfrac{\mu}{2\alpha\beta^2}$

then solve equation (4.15)

if $\mu \geq \bar{\mu}_c$ then solve equation(4.16)

**In phase 2**

$$||\nabla\phi||^2 - \beta^2||\text{dev sym}\nabla u||^2 > \frac{\mu}{2\alpha\beta^2}$$

solve equation (4.15) and equation (4.16)

**In phase 3**

$$\text{if } ||\nabla\phi||^2 \leq \beta^2||\text{dev sym}\nabla u||^2 - \frac{\mu}{2\alpha\beta^2}$$

then solve equation (4.15)

If$\mu \geq \bar{\mu}_c$ then solve equation(4.16)

**Step 7:** Check convergence,

if $|\pi_{lin}(u_{n+1}^{i+1})| \leq$ tol

and $|\pi_{ang}(u_{n+1}^{i+1}) \leq$ tol, then

Increment the loading step time as $t_{n+1} \to t_n$ and move to Step 2

else

Increment the iteration $i + 1 \to i$

and then go to Step 3.

## 4.3 Numerical Results and Discussion

The potential distribution of microstructure in two particular scenarios is examined using the material model as introduced in Chapter 3.

In the first place, the material's microstructure is observed using a square plate with a central hole. In the second place the microstruture distribution in a Couette shear cell is investigated.

### 4.3.1 Formation of Localized Zones in a Perforated Square Domain under Pure Tension.

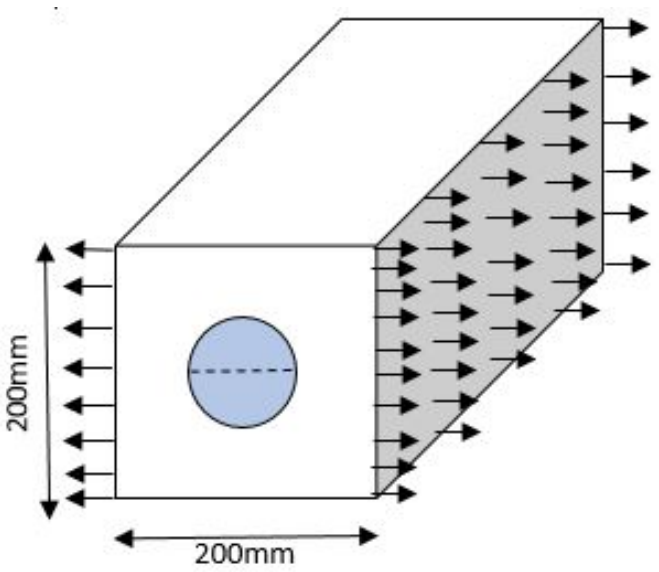


(a)

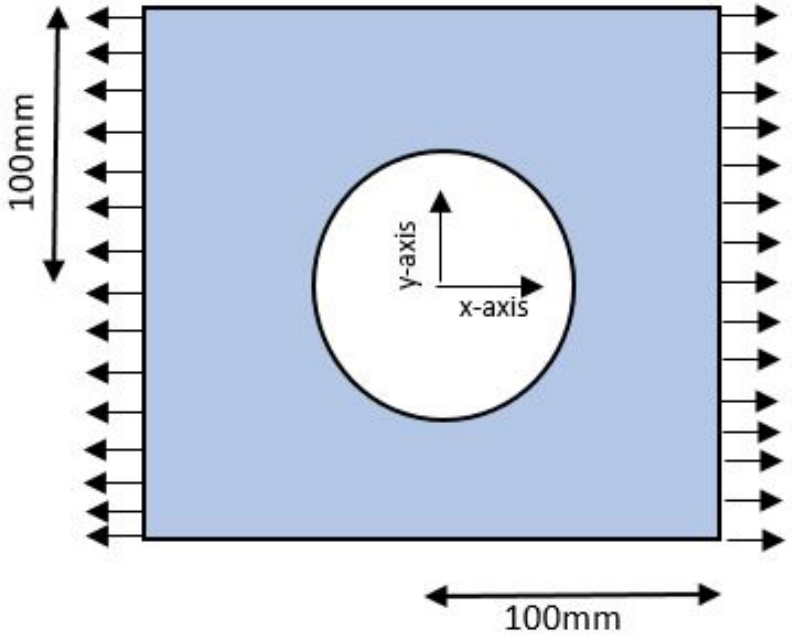


(b)

FIGURE 4.1: (a)Loading circumstances on the brick specimen's centeral hole geometry,
(b)symmetrical loading situations, which results in a reduced domain.

In this, we examine the elastic Cosserat material model's behavior, which was introduced in Chapter 3, by using an infinitely long granular brick specimen as

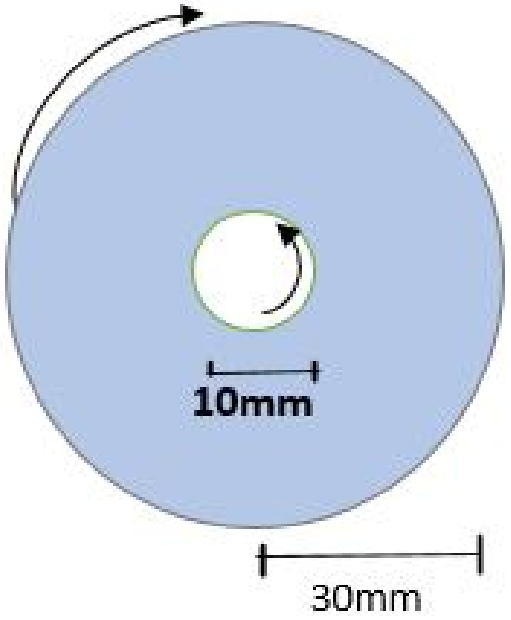


FIGURE 4.2: Schematic of the Couette shear cell under pure rotation.

shown in Figure 4.1(a) that has a central circular hole. The geometry of the problem and the associated loading conditions are illustrated in Figure 4.1. This setup allows us to apply plane strain conditions for implementing the model through a finite element scheme. To do this, we choose a perforated square plate with a unit thickness as the brick specimen's cross-section because of the symmetrical loading conditions, as depicted in Figure 4.1(b). Further, given the problem's symmetry, we only analyze one-fourth of the plate under a tension test. After that, the selected domain is divided into finite components.

The material constants utilized in the computations are listed in Table 4.1. We employ the finite element method to resolve the set of nonlinear equilibrium differential equations that resulted from the suggested model's two-field variational formulation, which was covered in the preceding chapter. The specimen is subjected to a displacement-controlled loading with a loading step of $1.0 \times 10^{-2}$, reaching a maximum of $17mm$ displacement.

The stopping criteria of the computational steps in the Newton-Raphson iteration procedure is used with a tolerance of $1.0 \times 10^{8}$.

To get Figure 4.3, the domain is discretized into 25883 number of finite elements that comprises 13192 number of vertices.

According to the numerical simulation results, the material exhibits a microstructure that is defined by the continuum particles' translational motions.
Figure 4.3 illustrates the distribution of the material's microstructural and non-microstructural areas.

TABLE 4.1: Material Parameters

| $E$ | $\nu$ | $\mu_c$ | $\bar{\lambda}$ | $\bar{\mu_c}$ | $\alpha$ | $\bar{\mu}$ | $\beta$ |
|---|---|---|---|---|---|---|---|
| $2.1\times10^4$ | 0.3 | 167 | 50 | 20 | 500 | 20 | 15 |

It is seen that the regions of the material experiencing highest stresses transition into the microstructural phase, where the continuum particles translate. In the perforated square plate, a distinct development of the localized deformation bands that originate from the entire is observed in the Figure 4.3(b). This formation of the localized shear band is due to the underlying microstructure in the medium and this is highly due to the localized shear strains in the medium. This shows that the presented model is capable of predicting the localized zones in the medium that are leading to the plastic deformation afterwards while being in the limit of elasticity.

The horizontal and vertical displacement fields are drawn at different simulation times in the given Figures 4.4 and 4.5. It can be seen that the formation of the localized zone develop with the passage of time and propagate within the medium where the localized shear is more dominant.

TABLE 4.2: Material Parameters while varying $\mu_c$

| $E$ | $\nu$ | $\mu_c$ | $\bar{\lambda}$ | $\bar{\mu_c}$ | $\alpha$ | $\bar{\mu}$ | $\beta$ |
|---|---|---|---|---|---|---|---|
| $2.1\times10^4$ | 0.3 | 163 | 50 | 20 | 500 | 20 | 15 |
| $2.1\times10^4$ | 0.3 | 167 | 50 | 20 | 500 | 20 | 15 |
| $2.1\times10^4$ | 0.3 | 173 | 50 | 20 | 500 | 20 | 15 |

In 4.7, the curves shows load-displacement for different values of the material

parameter $\mu_c$ are presented, but these curves' slopes with the designated displacement are shown.

This figures not only show the evolution of the material's microstructure as the values of $\mu_c$ change, as shown in 4.2, but they also reveal the nonlinear behavior of the Cosserat tangent modulus in the regime of non-microstructures and remains linear (with a fixed value) in the regime of microstructures of the material.

The influence of Cosserat coupled modulus $\mu_c$ is shown in 4.7. In this figure the evolution of horizontal and vertical displacements along the $x$ and $y$ directions in the mid section of the material domain are shown. It can be seen that the horizontal displacements are affected and increased with increasing value of the Cosserat coupled modulus in the region where there is no microstructure in the medium.

Whereas, in the region where there is a microstructure and a localized shear band is formed the Cosserat coupled modulus do not affect the horizontal and vertical displacements too significantly.

### 4.3.2 Formation of Localized Zones in a Couette Shear Cell under Pure Rotation.

The development of a test that causes strong rotations among the material particles is required in order to examine all of the non-microstructural and microstructural phases in the material. This test can greatly increase the rotational influence on the strain energy of the material.

Two forms of particle rotations—counter rotations and identical rotations—are shown in 4.2, which illustrates the kinematics of particle rotations. The suggested interaction energy potential is strongly rotated by the rotational effect of counter-rotating particles.

On the other hand, identical rotations of particles mostly result in a sliding impact on the interaction energy potential. The phenomena of particle rotations depends

on the particle size in a constrained geometry and under certain boundary conditions.

The study focuses on the formation of microstructure within a Couette annular geometry utilizing the proposed model. Couette geometries have been employed in experiments to analyze shear flows in granular materials. Imagine a granular material confined between two concentric rigid circular cylinders. These cylinders rotate in opposite directions.

To simplify the analysis, we only consider the first quadrant of the annular plate for observing microstructure formation. The annular domain experiences in-plane shear deformation due to the rotational motions applied at the outer boundaries.

The inner circular boundary is placed 10 mm from the annulus's origin, and the annular' breadth is fixed at 20 mm. Because the circular boundaries are made to revolve in opposing directions, the particles inside the annular domain rotate in two different ways. For the numerical simulation utilizing the suggested model, the boundary conditions involve fixed displacement along the circular boundaries, while a micromotion of one radian is applied at the boundaries.

The stopping criteria of the computational steps in the Newton-Raphson iteration procedure is used with a tolerance of $1.0 \times 10^8$. Examining the creation of microstructural phases in the annular domain subjected to rotational deformation is the goal of this work.

As the particles move both translationally and micro-rotationally, we see the development of microstructures. In Figure 4.8(c), the material displays a microstructure related to the micro-rotations of the continuum particles. Figures 4.8(a), 4.8(b), 4.8(c) and 4.8(d) demonstrate that for specific values, the material exhibits microstructures in both translational and micro-rotational particle motions.

In 4.9, the behavior of coupled shear modulus is given along x-axis. Those curves gives us the width of band. Hence, it indicates that all material phases can coexist. Furthermore, as the particle size decreases, the microstructure in the micromotions of the particles becomes more pronounced.

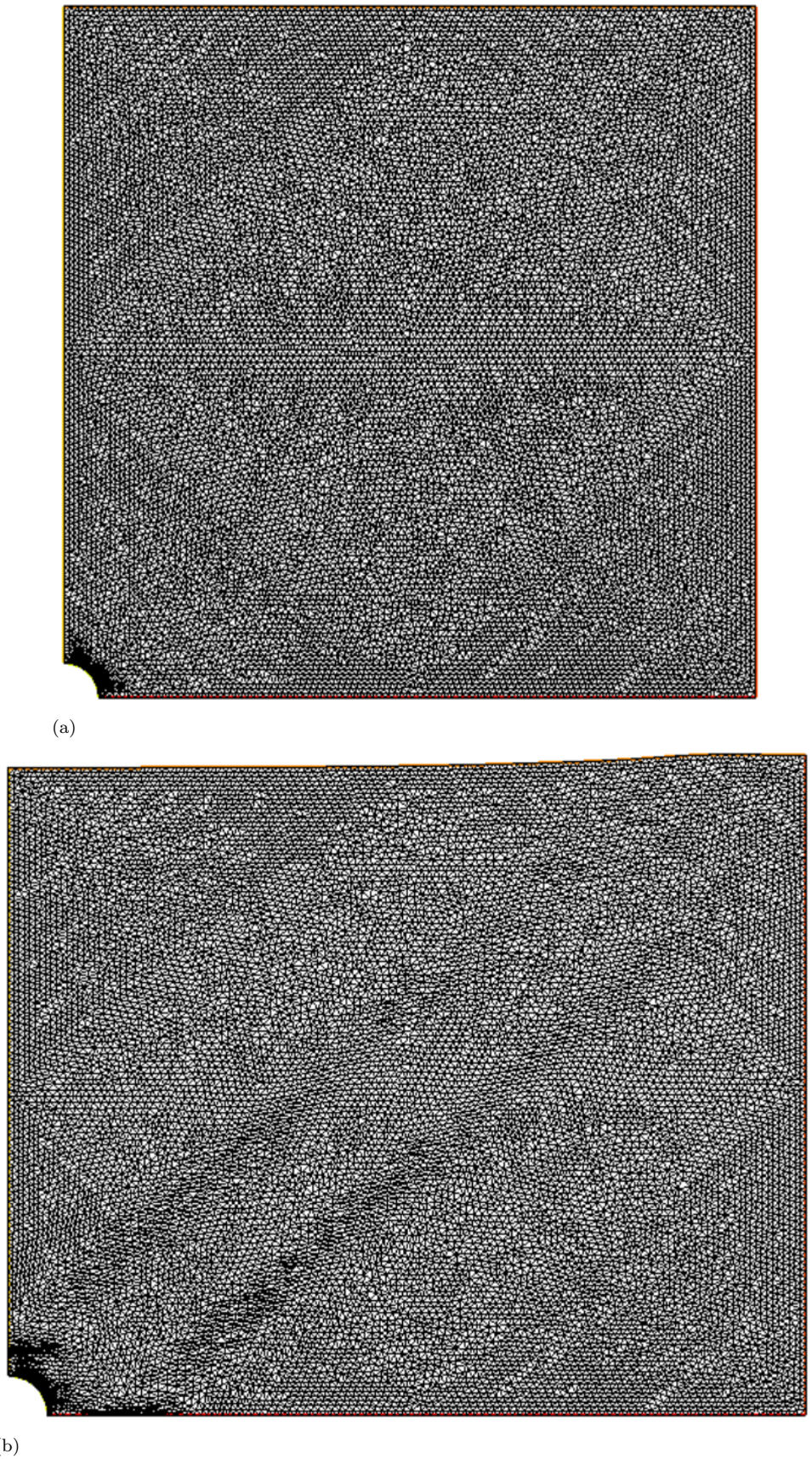

(a)

(b)

FIGURE 4.3: Formation of localized zones within an elastic material under tension. In the subfigure (a) undeformed configuration of the material and in the subfigure (b) the deformed configuration is shown.

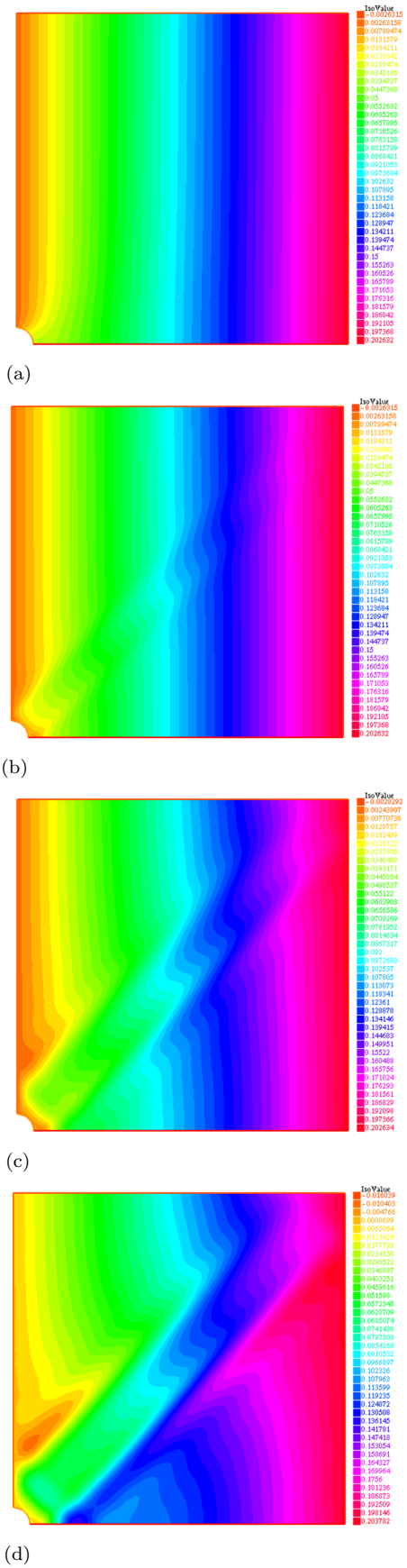

(a)

(b)

(c)

(d)

FIGURE 4.4: Horizontal displacement field within the elastic medium under pure tension. At the simulation time (a) $t = 0.1$, (b) $t = 0.5$, (c) $t = 0.75$ and (d) $t = 1$.

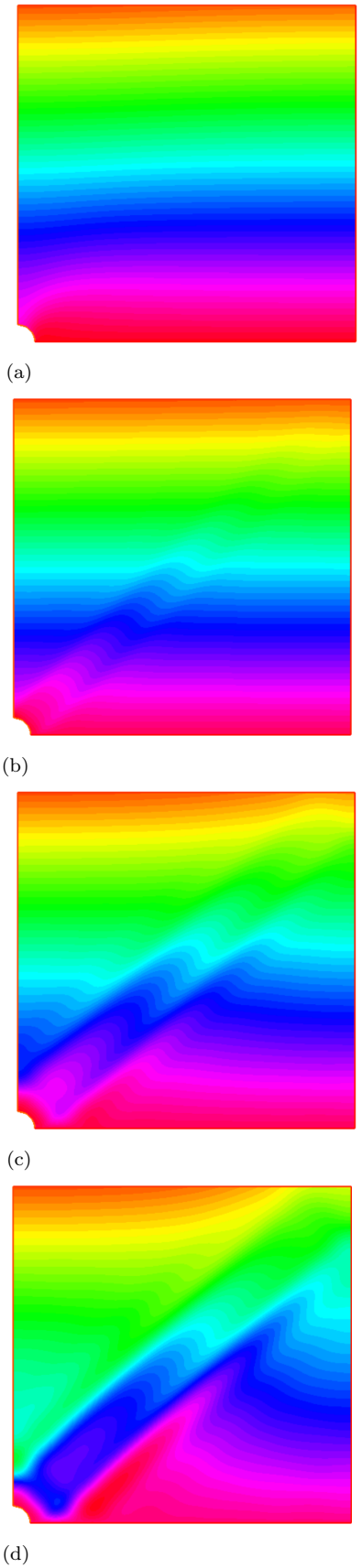

(a)

(b)

(c)

(d)

FIGURE 4.5: Vertical displacement field within the elastic medium under pure tension. At the simulation time (a) $t = 0.1$, (b) $t = 0.5$, (c) $t = 0.75$ and (d) $t = 1$.

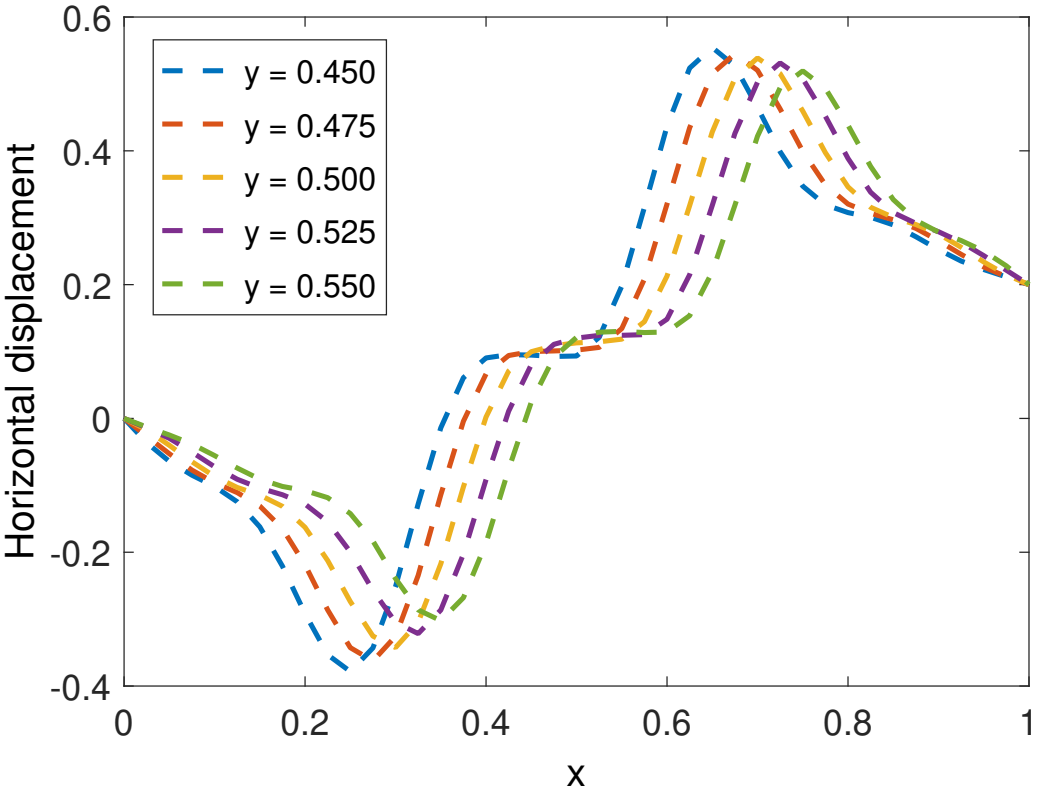


(a)

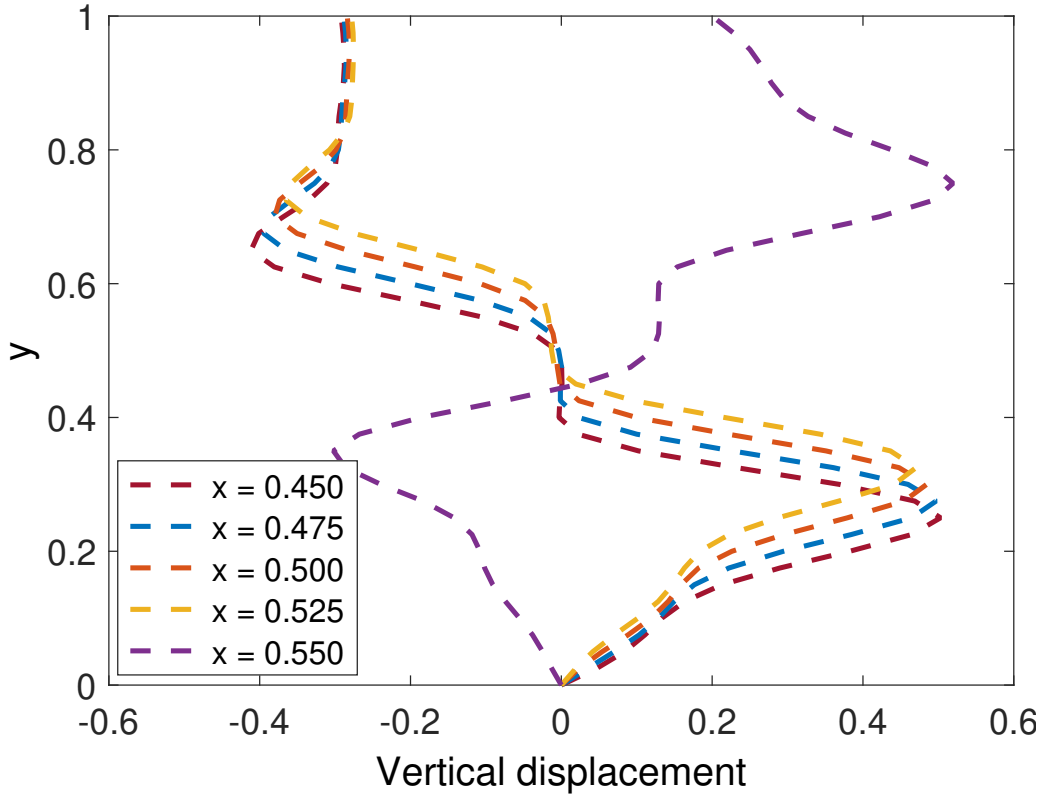


(b)

FIGURE 4.6: The material parameters used here are $E = 2.1 \times 10^5$, $\nu = 0.3$, $\alpha = 500$, $\mu_c = 167$, $\mu_o = 20$, $\beta = 15$, $\bar{\lambda} = 50$, $\bar{\mu_c} = 20$, $\bar{\mu} = 30$. At (a) Horizontal displacements along $x$ and (b) Vertical displacements along $y$

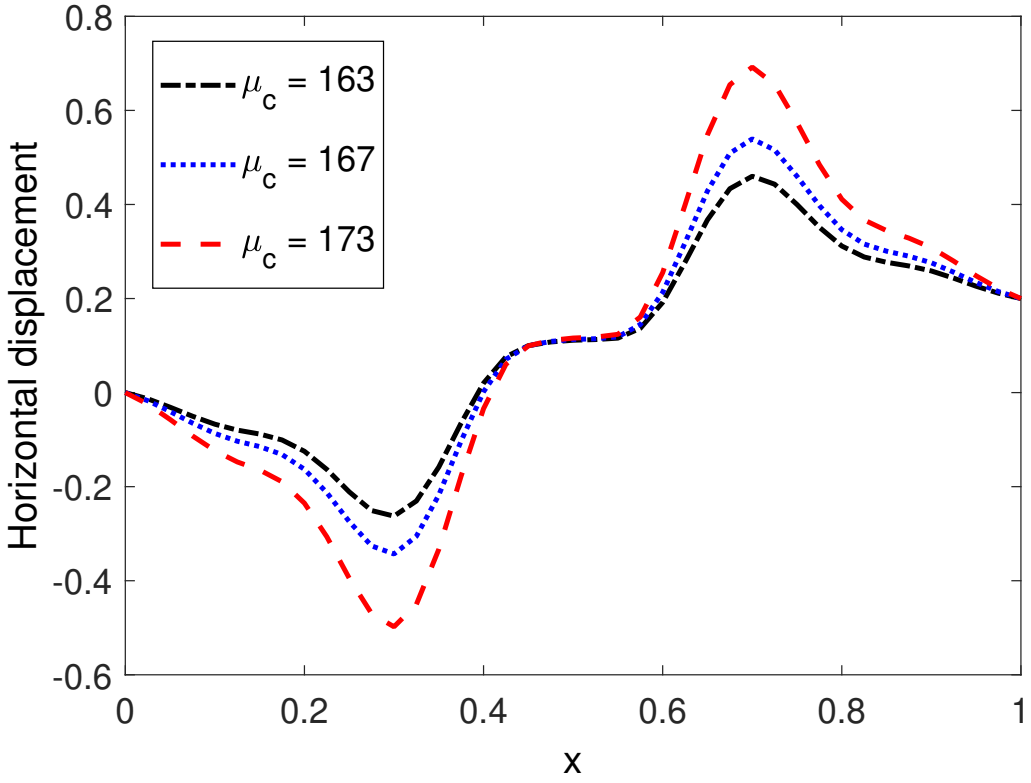


(a)

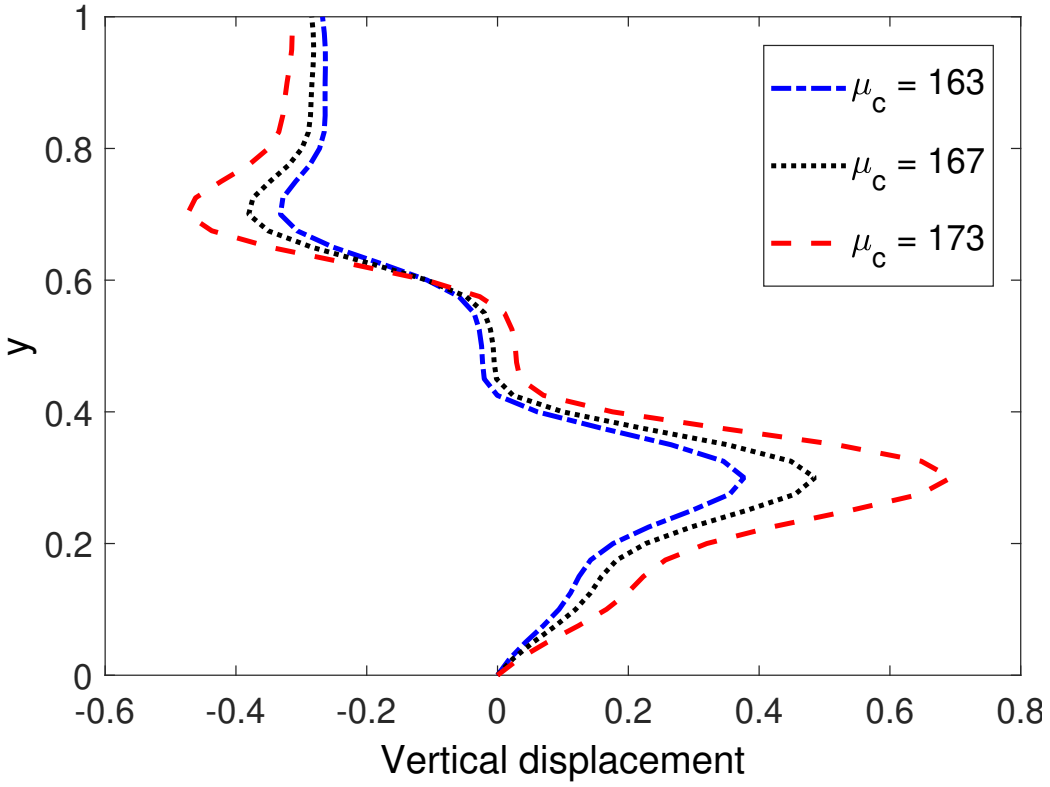


(b)

FIGURE 4.7: The material parameters used here are $E = 2.1 \times 10^5$, $\nu = 0.3$, $\alpha = 500$, $\mu_o = 20$, $\beta = 15$, $\bar{\lambda} = 50$, $\bar{\mu_c} = 20$, $\bar{\mu} = 30$. At (a) Horizontal displacements along $x$ for varying $\mu_c$ and (b) Vertical displacements along $y$ for varying $\mu_c$.

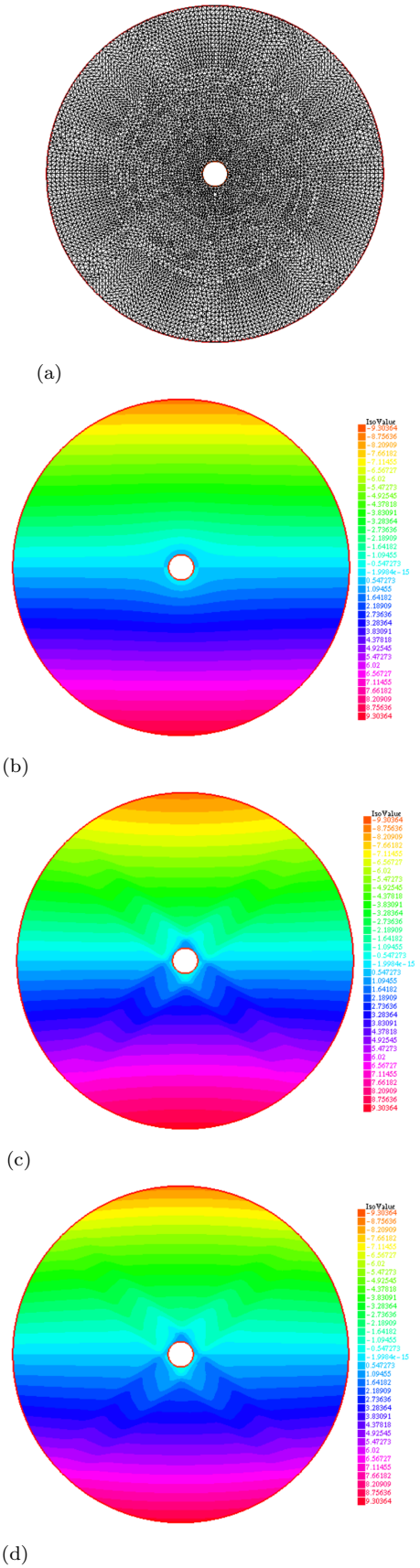

(a)

(b)

(c)

(d)

FIGURE 4.8: Horizontal displacement field within the annular domain under pure rotation. At the simulation time (a) $t = 0.1$, (b) $t = 0.5$, (c) $t = 0.75$ and (d) $t = 1$.

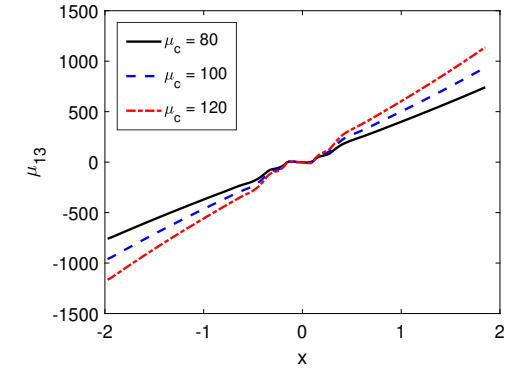


(a)

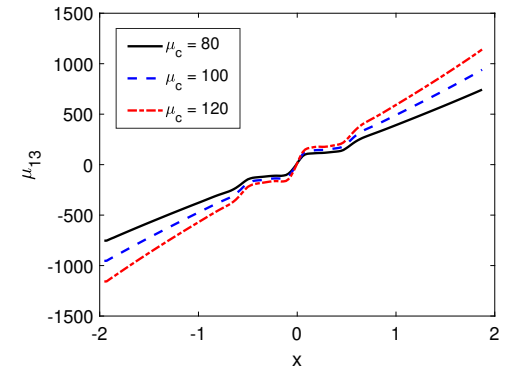


(b)

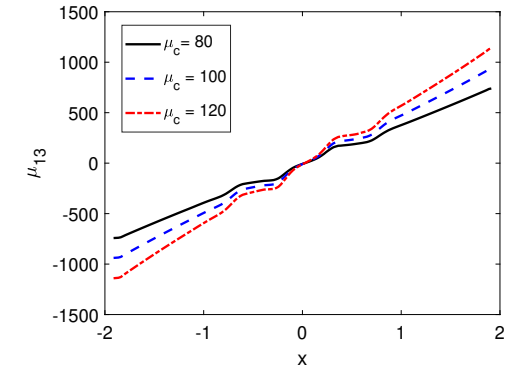


(c)

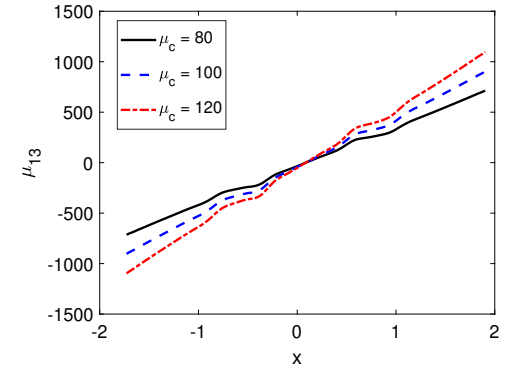


(d)

FIGURE 4.9: The material parameters used here are $E = 2.1 \times 10^5$, $\nu = 0.28$, $\alpha = 6.7 \times 10^3$, $\mu_c = 1.2 \times 10^2$, $\mu_0 = 22$, $\beta = 20$, $\bar{\lambda} = 20$, $\bar{\mu}_c = 5.0 \times 10^2$, $\bar{\mu}_0 = 80$. At the simulation time (a)$t = 0.1$, (b) $t = 0.5$, (c) $t = 0.75$ and (d) $t = 1$.

# Chapter 5

# Conclusion and Future Work

In this thesis we introduce a relaxed continuum model for granular structures that enables predicting the formation of localized deformations within the structure. A relaxed energy potential in the Cosserat continuum serves as a description of the mathematical model shown. The constitutive response of the elastic material in question is then determined using this energy potential. We can capture the localized deformation bands that emerge within the granular structure when stress is applied due to the model described. Localized medium deformations caused by fine-scale oscillations of the underlying microstructure in the elastic medium cause granular bands to form in the structured material. The model that was presented in the elastic regime is then converted into a finite element setting and put into practice using the FreeFEM++ open source tool. Two test issues in structural mechanics are analyzed using the implemented code. The compression of a granular slab under pure compression is the first problem that has been considered, and the Couette shear cell under pure rotation is the second problem that was analyzed for the localized deformation band formation. The results are displayed for both scenarios, where the implemented code demonstrates microstructure creation and associated shear band formation.

In the future, the analysis presented can be further extended to three dimension problem, enabling the modeling and simulation of localized deformation zones within complex elastic structures. The potential applications of the presented

model is in the modeling of granular soil structures. The model can be applied to simulate the failure of granular soil structures under load-bearing capacity problems. A natural extension of the presented formulation can be used to model and simulate localized deformation zones within three-dimensional elastic structures. Localized deformation zones within three-dimensional elastic structures refer to areas where the material undergoes significant deformation, often leading to failure or instability. Deformation is concentrated in a specific region, rather than being evenly distributed throughout the structure. Localized deformation zones often coincide with areas of high stress, which can lead to material failure. Deformation patterns can be complex and non-uniform, making it challenging to predict and analyze. In materials like metals or ceramics, localized deformation zones can form around cracks, leading to propagation and potentially catastrophic failure. In ductile materials, localized deformation zones can manifest as shear bands, where the material deforms severely, leading to strain softening. In slender structures, localized deformation zones can occur due to buckling, where the structure deforms excessively, leading to instability. Understanding localized deformation zones is crucial in various fields. In materials science, it is important for developing materials with improved strength and durability. Thus above applications highlights the versatility and potential of the presented model for future research and simulations.

# Bibliography


[1] B.L. Adams, M. Lyon, and B. Henrie. Microstructures by design: linear problems in elastic–plastic design. *International Journal of Plasticity*, 20(8): 1577–1602, 2004.

[2] S. Govindjee, K. Hackl, and R. Heinen. An upper bound to the free energy of mixing by twin-compatible lamination forn-variant martensitic phase transformations. *Continuum Mech. Therm.*, 18:443–553, 2007.

[3] M.S. Khan and K. Hackl. Modeling of microstructures in a cosserat continuum using relaxed energies. *Applications of Mathematics to Mechanics*, 27, 2018.

[4] S. Kumar, A. Vidyasagar, and D. M. Kochmann. An assessment of numerical techniques to find energy-minimizing microstructures associated with nonconvex potentials. *International journal for Numerical methods in engineering*, 2019.

[5] J. Voss, R.J. Martin, and O. Sander et al. Numerical approaches for investigating quasiconvexity in the context of morrey's conjecture. *Journal of non linear science*, 2022.

[6] J. Voss, R.J. Martin, and O. Sander et al. The quasiconvex envelope of conformally invariant planar energy functions in isotropic hyperelasticity. *Journal of non linear science*, 2020.

[7] J.R. Mianroodi, P. Shanthraj, and C. Liu et al. Modeling and simulation of microstructure in metallic systems based on multi-physics approaches. *npj Comput Mater 8*, 93, 2022.

[8] M. Massoudi. Remarks on constitutive modeling of granular materials. *Eng 4*, 4:2856–2878, 2023.

[9] A Haeri and K. Skonieczny. Three-dimensionsal granular flow continuum modeling via material point method with hyperelastic nonlocal granular fluidity. *Computer Methods in Applied Mechanics and Engineering*, 394:114904, 2022. ISSN 0045-7825. doi: https://doi.org/10.1016/j.cma.2022.114904.

[10] L. Borkowski, M. Anahid, A. Staroselsky, and W. Hu. Microstructure-sensitive large-deformation model for thermomechanical processing simulations. *International Journal of Solids and Structures*, 230-231:111161, 2021. ISSN 0020-7683. doi: https://doi.org/10.1016/j.ijsolstr.2021.111161. URL https://www.sciencedirect.com/science/article/pii/S0020768321002511.

[11] Lyesse Laloui and Alessandro F. Rotta Loria. Chapter 4 - deformation in the context of energy geostructures. In L. Laloui and A.F. Rotta Loria, editors, *Analysis and Design of Energy Geostructures*, pages 137–205. Academic Press, 2020. ISBN 978-0-12-820623-2. doi: https://doi.org/10.1016/B978-0-12-816223-1.00004-7.

[12] P. Surówka, A. Souslov, F. Jülicher, and D. Banerjee. Odd cosserat elasticity in active materials. *Phys. Rev. E*, 108, 2023.

[13] J.F. Ganghoffer, I. Goda, and R. Rahouadj. Size-dependent dynamic behavior of trabecular bone. In *Multiscale Biomechanics*, pages 317–344, 2018.

[14] P. Poorsolhjouy and A. Misra. Granular micromechanics based continuum model for grain rotations and grain rotation waves. *Journal of the Mechanics and Physics of Solids*, 129:244–260, 2019. ISSN 0022-5096. doi: https://doi.org/10.1016/j.jmps.2019.05.012.

[15] T.B. Trinch and K.Hackl. Modelling of shear localization in solids by means of energy relaxation. *Asia Pacific Journal on Computational Engineering*, pages 1–9, 2014.

[16] H. Tang and C. Song. Cosserat continuum model and its application to the studies of progressive failure. *Japanese Geotechnical Society Special Publication*, 2:703–708, 2016.

[17] D. Tanner and C. Brandes. Fault mechanics and earthquakes. In *Understanding Faults*, pages 11–80, 2020.

[18] SMJ Seyedan. *Granular Material Point Method: a numerical approach based on continuum mechanics for modelling granular flows.* PhD thesis, Aalto University, 01 2023.

[19] W. Dai, D. Hanaor, and Y. Gan. The effects of packing structure on the effective thermal conductivity of granular media: A grain scale investigation. *International Journal of Thermal Sciences*, 142:266–279, 2019. ISSN 1290-0729. doi: https://doi.org/10.1016/j.ijthermalsci.2019.04.028. URL https://www.sciencedirect.com/science/article/pii/S1290072918315758.

[20] N. Yilmaz, M.E. Yildizdag, F. Fabbrocino, L. Placidi, and A. Misra. Emergence of critical state in granular materials using a variationally-based damage-elasto-plastic micromechanical continuum model. *International Journal for Numerical and Analytical Methods in Geomechanics*, 48, 2024.

[21] F. Nicot, A. Wautier, and J. Lerbet. Hyperelastic or hypoelastic granular circular chain instability in a geometrically exact framework. *Journal of Engineering Mechanics*, 148(9):04022053, 2022.

[22] Y. Xu, J. Zhang, Y. Bai, and M. A. Meyers. Shear localization in dynamic deformation: Microstructural evolution. *Metallurgical and Materials Transactions*, 39:811–843, 2008.

[23] P. Frint and et al. Microstructural evolution during severe plastic deformation by gradation extrusion. *Metals 8*, 2:96, 2018.

[24] U. Ali et al. Role of particle rotation in sheared granular media. *Acta Geotech.*, 18:4599–4614, 2023.

[25] C. Xiu and X. Chu. Finite element simulations on failure behaviors of granular materials with microstructures using a micromechanics-based cosserat elastoplastic model. *Computer Modeling in Engineering & Sciences*, 138(3): 2305–2338, 2024. URL http://www.techscience.com/CMES/v138n3/54930.

[26] C.J. Akisin, C.J. Bennett, F. Venturi, H. Assadi, and T. Hussain. Numerical and experimental analysis of the deformation behavior of cocrfenimn high entropy alloy particles onto various substrates during cold spraying. *J Therm Spray Tech*, 31:1085–1111, 2022.

[27] R. Ge and Q. Liu. Digital design and manufacturing of microstructural granular materials. *Digital Engineering*, 2:100008, 2024. ISSN 2950-550X. doi: https://doi.org/10.1016/j.dte.2024.100008. URL https://www.sciencedirect.com/science/article/pii/S2950550X24000086.

[28] M. Wu, Z. Xia, and J. Wang. Constitutive modelling of idealised granular materials using machine learning method. *Journal of Rock Mechanics and Geotechnical Engineering*, 15(4):1038–1051, 2023. ISSN 1674-7755. doi: https://doi.org/10.1016/j.jrmge.2022.08.002. URL https://www.sciencedirect.com/science/article/pii/S1674775522001688.

[29] J. Chang, X. Chu, and Y. Xu. Finite-element analysis of failure in transversely isotropic geomaterials. *International Journal of Geomechanics*, 15(6): 04014096, 2015.

[30] S.D.C. Walsh and A. Tordesillas. Finite element methods for micropolar models of granular materials. *Applied Mathematical Modelling*, 30:1043–1055, 10 2006. doi: 10.1016/j.apm.2005.05.016.

[31] A. Amoddeo and P. Giovine. Micromechanical modelling of granular materials and fem simulations. *Meccanica*, 54, 12 2018. doi: 10.1007/s11012-018-00927-8.

[32] A. Holzapfel and Gerhard. Chapter 1 - introduction to vectors and tensors. In *Nonlinear Solid Mechanics A Continuum Approach for Engineering*. Copyright, 2000. doi: http://10.6.20.12:80/handle/123456789/46227.

[33] J. Stewart. Chapter 16- vector fields. In *Calculus: Early Transcendentals, 8th Edition*. Cengage Learning, 2015.

[34] J.M. Lee. Chapter 10-tensors. In *Introduction to Smooth Manifolds*. Springer, 2013.

[35] H.L. Royden and P. Fitzpatrick. *Chapter 6- Lp spaces*. Pearson, 2010.

[36] L.C. Evans. Chapter 5-sobolev spaces. In *Partial Differential Equations*. American Mathematical Society, 2010.

[37] M.S. Khan. On the observation of extended microstructures and localized deformations in granular materials-a feature of excat quasi-convex energy envelope. *Latin American Journal of Solids and Structures*, 03 2019. doi: 10.1590/1679-78255419.